

## Effects of initial stresses on guided wave propagation in multilayered PZT-4/PZT-5A composites: A polynomial expansion approach



Cherif Othmani<sup>a</sup>, He Zhang<sup>a</sup>, Chaofeng Lü<sup>a,b,c,\*</sup>

<sup>a</sup> College of Civil Engineering and Architecture, Zhejiang University, Hangzhou 310058, China

<sup>b</sup> Key Laboratory of Soft Machines and Smart Devices of Zhejiang Province, Zhejiang University, Hangzhou 310027, China

<sup>c</sup> Soft Matter Research Center, Zhejiang University, Hangzhou 310027, China

### ARTICLE INFO

#### Article history:

Received 7 December 2018

Revised 12 September 2019

Accepted 2 October 2019

Available online 15 October 2019

#### Keywords:

Guided wave propagation

Lamb and SH waves

Initial stresses

Legendre polynomial method

### ABSTRACT

Effects of initial stresses on the dispersion curves of Lamb and SH waves in multilayered PZT-4/PZT-5A composites are investigated using the polynomial expansion approach. The piezoelectric layers are considered with arbitrary crystal orientations with a result that only Lamb or SH waves may be transmitted. The problem is solved employing the Legendre polynomial approach that poses the advantages of numerically stability and effectiveness over conventional matrix method. The solution is validated by comparing the wave propagation behavior of piezoelectric materials with those reported in literature, and the convergence properties are examined. Numerical results demonstrate that initial stress has profound influences on the guided wave propagation in multilayered PZT-4/PZT-5A laminates. The phase velocity of Lamb and SH waves increases with initial tensile stresses. In addition, the effects of initial stresses rely on the wave mode and thickness of constituent layers and the stacking sequence of the constituent materials. The results are useful for understanding and optimization of new designs for actuator, electromechanical sensor and acoustic wave devices made of PZT-4/PZT-5A composites.

© 2019 Published by Elsevier Inc.

## 1. Introduction

Smart materials have received intensive attentions from the scientific community since the past decades with strong focuses on application of ultrasonic transducer and MEMS. In this area, piezoelectric materials have great promise for composing intelligent devices and structures. In general, the piezoelectric effect, firstly discovered by the brothers Curie in 1880 [1], is the phenomenon that characterizes the capacity of certain crystals or materials to convert mechanical pressure into electrical voltage and vice versa. Research works regardless of computational or experimental aspects on guided waves propagation in multilayered piezoelectric structures have brought about several challenging problems that are attracting intensive attention [2–6]. Among these, the propagation of acoustic waves in sandwich piezoelectric structures have been a subject of intensive numerical researches [7] and have been applied in several areas of engineering sciences [8,9]. Composite sandwich structures consisting of stack of different materials are widely used due to their specific proprieties that are unavailable in simple homogeneous structures. Consequently, this structure can be easily designed to meet technical requirements. In

\* Corresponding author at: College of Civil Engineering and Architecture, Zhejiang University, Hangzhou 310058, China.  
E-mail address: [lucf@zju.edu.cn](mailto:lucf@zju.edu.cn) (C. Lü).

addition, there has been growing application and demand for control elements involving piezoelectric devices in high technology industry such as actuators in active control, ultrasonic generators, filters and sensors in signal processing, etc. At that point, numerical knowledge of guided wave behaviors in sandwich structures gives insight into the design of these composite structures and improves their performance for various applications. Owing to the great variety of composite structure geometries and related type of acoustic waves, solving these categories of problems always encounters numerical processes. Moreover, the propagation of acoustic waves in finitely deformed electroelastic and magnetoelastic solids in the presence of an initial uniform magnetic field was addressed by Saxena and Ogden [10–12].

Because of the dissimilar materials proprieties, the individual layers are usually subjected to high internal residual stresses since the layered piezoelectric structures are usually prestressed during manufacturing process and in service to avoid brittle fracture [13]. In this context, previous research has shown that the effect of initial stresses on acoustic wave propagation became favorable and is of great importance while taking up problems in the non-destructive testing of materials, mechanics of composite materials, bio-mechanics and rock mechanics. To date, many endeavors have been devoted to the analysis of initial stress effect on acoustic wave propagation. Zhou et al. [13] investigated the effects of initial stresses on bulk wave propagation in layered piezomagnetic/piezoelectric plates, with special focus on the phase velocities and frequency spectrum of bulk waves. Jie and Jinxiong [14] analyzed the effects of initial stress on propagation of Lamb waves in a thin plate. Son and Kang [15] studied numerically the effects of initial stress on the propagation behavior and dispersion relation of shear horizontal (SH) waves in piezoelectric plates. Guo and Wei [16], investigated the effects of initial stress on the reflection and transmission of waves at the interface between two piezoelectric half spaces. In the same context, Shams [17] demonstrated the effects of initial stress on phase velocities of surface Love wave in hetero-structures, while Singhal et al. [18] investigated a similar problem in piezo-composite structure composed of functionally graded piezoelectric material (FGPM).

Many approaches have been proposed to study the acoustic wave propagation and dynamics behavior of multilayered piezoelectric media. Among them, the transfer matrix method is one of the most favorable since it can deal with multilayered structures with high efficiency in a condensed matrix size irrespective of the number of layers. However, as pointed by many researchers [19,20], when it comes to acoustic wave propagation in multilayered piezoelectric structures, numerical instabilities arise frequently due to the presence of large value of the produce of frequency and transfer distance. Chen et al. [21] developed the state space method and the differential quadrature method to solve free vibration of beams resting on a Pasternak elastic foundation. Zheng et al. [22] used the local radial basis function collocation method for study the band structure computation of phononic crystals with scatterers of arbitrary geometry. Recently, Biswas and Abo-Dahab [23] used the Helmholtz's theorem to study the effect of phase-lags on Rayleigh wave propagation under initially stressed magneto-thermoelastic orthotropic medium. Moreover, for the stiffness matrix [24], numerical instabilities arise when applied for calculating the acoustic wave propagation in multilayered structures. Based on the matrix formalism, Takali et al. [25] presented the ordinary differential equation approach to study the surface acoustic waves propagation in the piezoelectric structures. They have shown that this method remains always stable numerically, but, the testing time is always long which results in highly computational costs. Comparatively, the global matrix method [20] is more numerically stable and consequently is often used as a benchmark solution to model piezoelectric layered media. However, it is also very complex due to the increasing matrix scale with layer number. In addition, the search of roots by these matrix formalisms is a difficult task, and sometimes part of the roots will probably be missed if the numerical strategy is improperly employed. Wang and Shen [26] present a detailed study of the fundamental understanding of guided wave mechanism in piezoelectric composite plates using finite element method (FEM) with Bloch–Floquet boundary condition (BFBC). This approach has been widely used to model dynamic response of guided wave in piezoelectric composite structures [26], which can provide accurate and computationally efficient solutions.

In 1998, polynomial method has been proposed by Lefebvre et al. [27] to solve surface wave propagation in the multilayered piezoelectric structures. This orthogonal function technique was extended by Yu et al. [28,29] who developed Legendre orthogonal polynomial method to solve the guided waves propagation in functionally graded structures. Recently, Othmani et al. [5–7,30–33] extended the Legendre polynomial method to study the propagation of Lamb and SH waves in anisotropic viscoelastic structure, piezoelectric and composite materials. The advantages of Legendre polynomial method mainly include the following aspects. Firstly, it automatically incorporates the mechanical boundary conditions in the Hooke's Law and Maxwell's equations. Secondly, it allows a numerical resolution by a non-iterative system to the eigenvalues and eigenvectors, that is, the final characteristic equations for eigenvalue are simple algebraic equation that corresponds to a single term of the Legendre polynomial expansion for displacement and electrical potential. Thirdly, the solution converges quickly with the truncated number due to the high convergence feature of the Legendre polynomial. This constitutes the most important advantage of this polynomial approach over most matrix formalisms.

In this paper, the influences of initial stress on propagation of Lamb and SH waves in multilayer piezoelectric composites is investigated using the Legendre polynomial method. The composites are composed of PZT-4 and PZT-5A crystals that are polarized in different orientations. The polarization directions are assumed [010; 001; 100] for SH waves, while [001; 100; 010] or [100; 010; 001] for Lamb waves. The original basic equations for different layers of the problem are firstly expressed in a uniform condensed manner by introducing the Heaviside step function, and then the displacements and electrical potential are expanded into the Legendre polynomial series. The governing characteristic equations are finally derived with the application of the orthogonality condition of modified Legendre polynomials. In numerical examples, the sensitivity of the guided waves propagation to the layer thickness and initial stress is intensively examined. The results

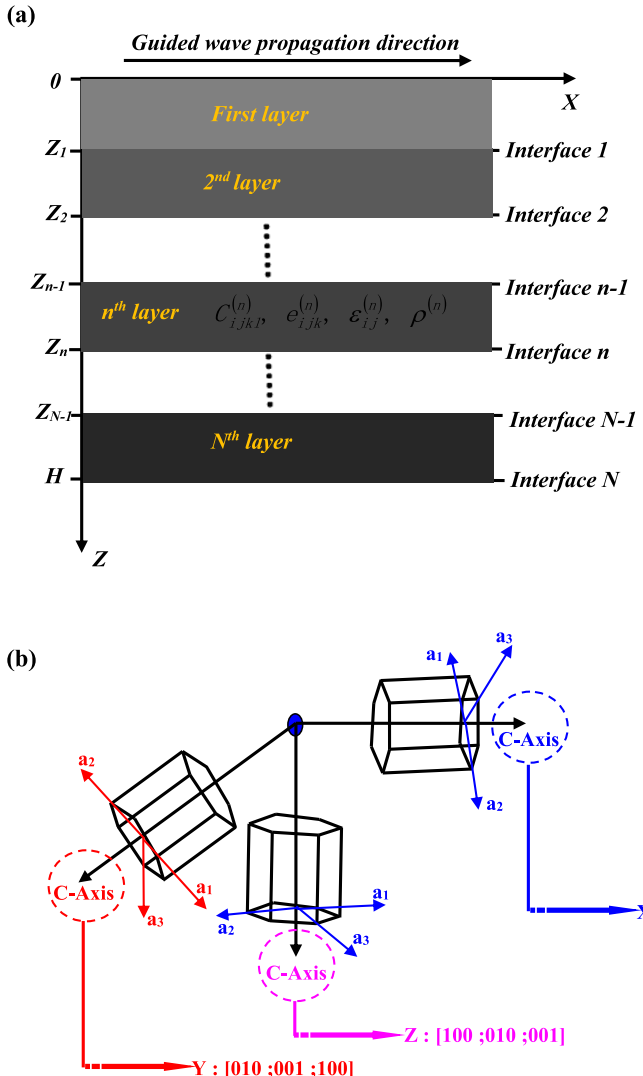


**Fig. 1.** (a) Schematic diagram expressed as of a piezoelectric multilayered structure showing in the coordinate system; (b) Hexagonal piezoelectric layers orientation.

suggest that the initial stress and laminate scheme may pose significant effects on the wave propagation characteristics and may be used as reference for the design of ultrasonic transducers for the detection of flaws in the industry non-destructive testing.

## 2. Theoretical formulations and solution

### 2.1. Basic equations

Consider a typical piezoelectric composites (total thickness  $H$ ) consisting of a perfect stacking of  $n$  homogeneous layers made of PZT4 and PZT5A (Fig. 1(a)). The Cartesian coordinate system ( $X$ ,  $Y$ ,  $Z$ ) is designated such that the plate, occupies the region  $0 \leq Z \leq H$  (Fig. 1(a)). It is assumed that the Lamb and SH- waves propagate along the positive direction of  $X$  axis. For SH waves, the polarization direction of each piezoelectric layers is along the  $Y$  axis, perpendicular to the  $X-Z$  plane and mentioned by  $[010; 001; 100]$ , while for Lamb waves, the piezoelectric layers are all polarized in the  $X$  or  $Z$  axes, prescribed respectively by  $[001; 100; 010]$  or  $[100; 010; 001]$  (Fig. 1(b)). Hence, the mechanical displacement and the electric potential, involves only the  $X$  and  $Z$  directions. The corresponding mathematical equations can also be found in many available data [34]. Here, it is assumed that the whole composites are endowed with a constant initial stress  $\sigma_X^0$  in the  $X$  direction, where the superscript “0” denotes the constant value of initial stress and “X” denotes its direction. Then, the field

equations governing wave propagation for piezoelectric materials can be expressed as [13]:

$$\frac{\partial \sigma_X}{\partial X} + \frac{\partial \tau_{XZ}}{\partial Z} + \sigma_0^X \frac{\partial^2 u_X}{\partial X^2} = \rho \frac{\partial^2 u_X}{\partial t^2} \quad (1a)$$

$$\frac{\partial \tau_{XY}}{\partial X} + \frac{\partial \tau_{YZ}}{\partial Z} + \sigma_0^Y \frac{\partial^2 u_Y}{\partial X^2} = \rho \frac{\partial^2 u_Y}{\partial t^2} \quad (1b)$$

$$\frac{\partial \tau_{XZ}}{\partial X} + \frac{\partial \sigma_Z}{\partial Z} + \sigma_0^Z \frac{\partial^2 u_Z}{\partial X^2} = \rho \frac{\partial^2 u_Z}{\partial t^2} \quad (1c)$$

$$\frac{\partial D_X}{\partial X} + \frac{\partial D_Z}{\partial Z} = 0 \quad (1d)$$

where  $\rho$  is the mass density,  $u_i$  and  $D_i$  denote respectively the mechanical and the electrical displacements in the  $i$ th direction.  $\sigma_i$  and  $\tau_{ij}$  are the normal and shear stresses. Obviously, Eq. (1b) is independent of the Eq. (1a) and (c). In fact, Eq. (1b) represents the propagation of SH wave in the piezoelectric composite, while Eq. (1a) and (c) controls the propagation of Lamb waves. Hence, in practice, the SH and Lamb guided waves will be separately dealt with.

The constitutive equations for piezoelectric crystals may differ according to the polarization direction and specific guided waves. Accordingly, the relationships of  $c_{ij}$  and  $c_{ijkl}$ ,  $e_{ij}$  and  $e_{ijk}$  are given in Appendix A. For SH wave with polarization [010; 001; 100],

$$\tau_{XY} = c_{66} \frac{\partial u_Y}{\partial X} + e_{16} \frac{\partial \phi}{\partial X} \quad (2a)$$

$$\tau_{YZ} = c_{44} \frac{\partial u_Y}{\partial Z} + e_{34} \frac{\partial \phi}{\partial Z} \quad (2b)$$

$$D_X = e_{16} \frac{\partial u_Y}{\partial X} - \varepsilon_{11} \frac{\partial \phi}{\partial X} \quad (2c)$$

$$D_Z = e_{34} \frac{\partial u_Y}{\partial Z} - \varepsilon_{33} \frac{\partial \phi}{\partial Z} \quad (2d)$$

where  $\phi$  is the electric potential. For Lamb wave with polarization [001; 100; 010],

$$\sigma_X = c_{11} \frac{\partial u_X}{\partial X} + c_{13} \frac{\partial u_Z}{\partial Z} + e_{11} \frac{\partial \phi}{\partial X} \quad (3a)$$

$$\tau_{XZ} = c_{55} \left( \frac{\partial u_Z}{\partial X} + \frac{\partial u_X}{\partial Z} \right) + e_{35} \frac{\partial \phi}{\partial Z} \quad (3b)$$

$$\sigma_Z = c_{31} \frac{\partial u_X}{\partial X} + c_{33} \frac{\partial u_Z}{\partial Z} + e_{13} \frac{\partial \phi}{\partial X} \quad (3c)$$

$$D_X = e_{11} \frac{\partial u_X}{\partial X} + e_{13} \frac{\partial u_Z}{\partial Z} - \varepsilon_{11} \frac{\partial \phi}{\partial X} \quad (3d)$$

$$D_Z = e_{35} \left( \frac{\partial u_Z}{\partial X} + \frac{\partial u_X}{\partial Z} \right) - \varepsilon_{33} \frac{\partial \phi}{\partial Z} \quad (3e)$$

For Lamb wave with polarization [100; 010; 001],

$$\sigma_X = c_{11} \frac{\partial u_X}{\partial X} + c_{13} \frac{\partial u_Z}{\partial Z} + e_{31} \frac{\partial \phi}{\partial Z} \quad (4a)$$

$$\tau_{XZ} = c_{55} \left( \frac{\partial u_Z}{\partial X} + \frac{\partial u_X}{\partial Z} \right) + e_{15} \frac{\partial \phi}{\partial X} \quad (4b)$$

$$\sigma_Z = c_{31} \frac{\partial u_X}{\partial X} + c_{33} \frac{\partial u_Z}{\partial Z} + e_{33} \frac{\partial \phi}{\partial Z} \quad (4c)$$

$$D_X = e_{15} \left( \frac{\partial u_Z}{\partial X} + \frac{\partial u_X}{\partial Z} \right) - \varepsilon_{11} \frac{\partial \phi}{\partial X} \quad (4d)$$

$$D_Z = e_{31} \frac{\partial u_X}{\partial X} + e_{33} \frac{\partial u_Z}{\partial Z} - \varepsilon_{33} \frac{\partial \phi}{\partial Z} \quad (4e)$$

In the above equations,  $c_{ijkl}$ ,  $e_{ijk}$  and  $\varepsilon_{jk}$  are respectively the elastic, piezoelectric and permittivity constants. For a plane harmonic wave propagating along the X-direction, the solution to the above governing equations may be assumed as:

$$\begin{pmatrix} u \\ \sigma_z \\ D_z \\ \tau_{xz} \\ \varphi \end{pmatrix} = \begin{pmatrix} H\bar{u}(\beta) \\ c_{55}^{(1)}\bar{\sigma}_z(\beta) \\ \sqrt{c_{55}^{(1)}\varepsilon_{33}^{(1)}}\bar{D}_z(\beta) \\ c_{55}^{(1)}\bar{\tau}_{xz}(\beta) \\ H\sqrt{\frac{c_{55}^{(1)}}{\varepsilon_{33}^{(1)}}}\bar{\varphi}(\beta) \end{pmatrix} e^{i(kX-\omega t)} \quad (5)$$

where,  $c_{55}^{(1)}$  and  $\varepsilon_{33}^{(1)}$  are the material constants of the PZT-4 layer,  $k$  the wave number,  $\omega$  the angular frequency, and  $i = \sqrt{-1}$  the imaginary unit. Then, Eq. (1) can be rewritten as:

$$\bar{k} \frac{\partial \bar{\sigma}_x}{\partial \alpha} + \bar{k} \frac{\partial \bar{\tau}_{xz}}{\partial \beta} + \bar{k}^2 \bar{\sigma}_0^x \frac{\partial^2 \bar{u}_x}{\partial \alpha^2} = -\bar{\rho}^{(n)} \Omega^2 \bar{u}_x \quad (6a)$$

$$\bar{k} \frac{\partial \bar{\tau}_{xy}}{\partial \alpha} + \bar{k} \frac{\partial \bar{\tau}_{yz}}{\partial \beta} + \bar{k}^2 \bar{\sigma}_0^y \frac{\partial^2 \bar{u}_y}{\partial \alpha^2} = -\bar{\rho}^{(n)} \Omega^2 \bar{u}_y \quad (6b)$$

$$\bar{k} \frac{\partial \bar{\tau}_{xz}}{\partial \alpha} + \bar{k} \frac{\partial \bar{\sigma}_z}{\partial \beta} + \bar{k}^2 \bar{\sigma}_0^z \frac{\partial^2 \bar{u}_z}{\partial \alpha^2} = -\bar{\rho}^{(n)} \Omega^2 \bar{u}_z \quad (6c)$$

$$\frac{\partial \bar{D}_x}{\partial \alpha} + \frac{\partial \bar{D}_z}{\partial \beta} = 0 \quad (6d)$$

where  $\alpha = kX$  and  $\beta = kZ$  are the non-dimensional coordinates,  $\bar{\rho}^{(n)} = \frac{\rho^{(n)}}{\rho^{(1)}}$  is the non-dimensional mass density, while  $\bar{k} = kH$  and  $\Omega = \omega H \sqrt{\frac{\rho^{(n)}}{c_{55}^{(1)}}}$  are the non-dimensional wave number and angular frequency with the superscript  $(n)$  denoting the  $n$ -th piezoelectric layer. The constitutive Eqs. (2)–(4) may also be rewritten in similar non-dimensional forms but are discarded here for brevity.

The boundary conditions at the upper and lower surfaces of the N-layered piezoelectric composites are

$$\bar{\tau}_{xz} = \bar{\tau}_{yz} = \bar{\sigma}_z = 0, \text{ (at } \beta = 0 \text{ and } \beta = kH \text{)} \quad (7a)$$

while the mechanical stresses and displacements should be continuous at the interfaces that read,

$$\begin{cases} \bar{u}_x(\beta_n^-) = \bar{u}_x(\beta_n^+), \bar{u}_y(\beta_n^-) = \bar{u}_y(\beta_n^+), \bar{u}_z(\beta_n^-) = \bar{u}_z(\beta_n^+) \\ \bar{\tau}_{xz}(\beta_n^-) = \bar{\tau}_{xz}(\beta_n^+), \bar{\tau}_{yz}(\beta_n^-) = \bar{\tau}_{yz}(\beta_n^+), \bar{\sigma}_z(\beta_n^-) = \bar{\sigma}_z(\beta_n^+) \end{cases} \quad (7b)$$

where the subscript denotes the  $n$ -th interface between the  $n$ -th and  $(n+1)$ -th layers. For representative illustrations, only open-circuit in vacuum is considered which requires the electric displacement to be zero at the upper and lower surfaces, i.e.,

$$\bar{D}_3 = 0, \text{ (at } \beta = 0 \text{ and } \beta = kH \text{)} \quad (7c)$$

The mechanical and electrical boundary and continuity conditions in Eq. (7) may be incorporated in the constitutive equations by introducing the rectangular window function  $\pi_{\beta_{n-1}, \beta_n}(\beta)$  [5–7,30–33], which takes 1 when  $\beta_{n-1} \leq \beta \leq \beta_n$  and 0 otherwise. For example, the boundary condition  $\bar{\tau}_{xz} = 0$  at the free surfaces  $\beta = 0$  and  $\beta = kH$  may be incorporated in the governing Eq. (6) by replacing  $\bar{\tau}_{xz}$  by  $\bar{\tau}_{xz} = \bar{\tau}_{xz}\pi_{0, kH}$ . Therefore, the term  $\frac{\partial \bar{\tau}_{xz}}{\partial \beta}$  should be replaced by  $\frac{\partial \bar{\tau}_{xz}}{\partial \beta}\pi_{0, kH} + \bar{\tau}_{xz}[\delta(0) - \delta(\beta - kH)]$ , where  $\delta(x - x_0)$  is the Kronecker delta function. With this rectangular window function, the discontinuous material constants for the multilayered composites can also be expressed in a condensed manner as [5–7]:

$$\aleph = \sum_{n=1}^N \aleph^{(n)} \pi_{\beta_{n-1}, \beta_n}(\beta), \quad (8)$$

where  $\aleph$  can be  $c_{ijkl}$ ,  $e_{ijk}$ ,  $\varepsilon_{jk}$  and  $\rho$ . For brevity, we use  $\pi_{\beta_{n-1}, \beta_n}$  to represent  $\pi_{\beta_{n-1}, \beta_n}(\beta)$  in the following text.

Substituting the solution of mechanical displacements and electric potential in Eq. (5) into the constitutive equations and then into the Eq. (6) with the aid of rectangular window function, the governing equation in terms of displacements are obtained as follows.

For the SH waves with polarization [010; 001; 100],

$$\begin{aligned} & -\bar{u}_Y \left[ \sum_{n=1}^N \bar{c}_{66}^{(n)} \pi_{\beta_{n-1}, \beta_n} + \bar{\sigma}_0^X \right] + \bar{u}'_Y \sum_{n=1}^N \bar{c}_{44}^{(n)} \pi'_{\beta_{n-1}, \beta_n} + \bar{u}''_Y \sum_{n=1}^N \bar{c}_{44}^{(n)} \pi_{\beta_{n-1}, \beta_n} - \bar{\phi} \sum_{n=1}^N \bar{e}_{16}^{(n)} \pi_{\beta_{n-1}, \beta_n} \\ & + \bar{\phi}' \sum_{n=1}^N \bar{e}_{34}^{(n)} \pi'_{\beta_{n-1}, \beta_n} + \bar{\phi}'' \sum_{n=1}^N \bar{e}_{34}^{(n)} \pi_{\beta_{n-1}, \beta_n} = -\left(\frac{\Omega}{k}\right)^2 \bar{u}_Y \sum_{n=1}^N \bar{\rho}^{(n)} \pi_{\beta_{n-1}, \beta_n} \end{aligned} \quad (9a)$$

$$\begin{aligned} & -\bar{u}_Y \sum_{n=1}^N \bar{e}_{16}^{(n)} \pi_{\beta_{n-1}, \beta_n} + \bar{u}''_Y \sum_{n=1}^N \bar{e}_{34}^{(n)} \pi_{\beta_{n-1}, \beta_n} - \bar{\phi} \sum_{n=1}^N \bar{\varepsilon}_{11}^{(n)} \pi_{\beta_{n-1}, \beta_n} + \bar{\phi}'' \sum_{n=1}^N \bar{\varepsilon}_{33}^{(n)} \pi_{\beta_{n-1}, \beta_n} + \bar{u}'_Y \sum_{n=1}^N \bar{e}_{34}^{(n)} \pi'_{\beta_{n-1}, \beta_n} \\ & + \bar{\phi}' \sum_{n=1}^N \bar{\varepsilon}_{33}^{(n)} \pi'_{\beta_{n-1}, \beta_n} = 0 \end{aligned} \quad (9b)$$

For Lamb wave with polarization [001; 100; 010],

$$\begin{aligned} & -\bar{u}_X \left[ \sum_{n=1}^N \bar{c}_{11}^{(n)} \pi_{\beta_{n-1}, \beta_n} + \bar{\sigma}_0^X \right] + \bar{u}'_X \sum_{n=1}^N \bar{c}_{55}^{(n)} \pi'_{\beta_{n-1}, \beta_n} + \bar{u}''_X \sum_{n=1}^N \bar{c}_{55}^{(n)} \pi_{\beta_{n-1}, \beta_n} + i\bar{u}_Z \sum_{n=1}^N \bar{c}_{55}^{(n)} \pi'_{\beta_{n-1}, \beta_n} - i\bar{u}'_Z \sum_{n=1}^N [\bar{c}_{55}^{(n)} + \bar{c}_{13}^{(n)}] \pi_{\beta_{n-1}, \beta_n} \\ & - \bar{\phi} \sum_{n=1}^N \bar{e}_{11}^{(n)} \pi_{\beta_{n-1}, \beta_n} + \bar{\phi}' \sum_{n=1}^N \bar{e}_{35}^{(n)} \pi'_{\beta_{n-1}, \beta_n} + \bar{\phi}'' \sum_{n=1}^N \bar{e}_{35}^{(n)} \pi_{\beta_{n-1}, \beta_n} = -\left(\frac{\Omega}{k}\right)^2 \bar{u}_X \sum_{n=1}^N \bar{\rho}^{(n)} \pi_{\beta_{n-1}, \beta_n} \end{aligned} \quad (10a)$$

$$\begin{aligned} & i\bar{u}_X \sum_{n=1}^N \bar{c}_{31}^{(n)} \pi'_{\beta_{n-1}, \beta_n} - i\bar{u}'_X \sum_{n=1}^N [\bar{c}_{55}^{(n)} + \bar{c}_{31}^{(n)}] \pi_{\beta_{n-1}, \beta_n} - \bar{u}_Z \left[ \sum_{n=1}^N \bar{c}_{55}^{(n)} \pi_{\beta_{n-1}, \beta_n} + \bar{\sigma}_0^X \right] + \bar{u}'_Z \sum_{n=1}^N \bar{c}_{33}^{(n)} \pi'_{\beta_{n-1}, \beta_n} + \bar{u}''_Z \sum_{n=1}^N \bar{c}_{33}^{(n)} \pi_{\beta_{n-1}, \beta_n} \\ & + i\bar{\phi} \sum_{n=1}^N \bar{e}_{13}^{(n)} \pi'_{\beta_{n-1}, \beta_n} - i\bar{\phi}' \sum_{n=1}^N [\bar{e}_{35}^{(n)} + \bar{e}_{13}^{(n)}] \pi_{\beta_{n-1}, \beta_n} = -\left(\frac{\Omega}{k}\right)^2 \bar{u}_Z \sum_{n=1}^N \bar{\rho}^{(n)} \pi_{\beta_{n-1}, \beta_n} \end{aligned} \quad (10b)$$

$$\begin{aligned} & -\bar{u}_X \sum_{n=1}^N \bar{e}_{11}^{(n)} \pi_{\beta_{n-1}, \beta_n} + \bar{u}'_X \sum_{n=1}^N \bar{e}_{35}^{(n)} \pi'_{\beta_{n-1}, \beta_n} + \bar{u}''_X \sum_{n=1}^N \bar{e}_{35}^{(n)} \pi_{\beta_{n-1}, \beta_n} + i\bar{u}_Z \sum_{n=1}^N [\bar{e}_{13}^{(n)} + \bar{e}_{35}^{(n)}] \pi_{\beta_{n-1}, \beta_n} + i\bar{u}_Z \sum_{n=1}^N \bar{e}_{35}^{(n)} \pi'_{\beta_{n-1}, \beta_n} \\ & - \bar{\phi} \sum_{n=1}^N \bar{\varepsilon}_{11}^{(n)} \pi_{\beta_{n-1}, \beta_n} + \bar{\phi}' \sum_{n=1}^N \bar{\varepsilon}_{33}^{(n)} \pi'_{\beta_{n-1}, \beta_n} + \bar{\phi}'' \sum_{n=1}^N \bar{\varepsilon}_{33}^{(n)} \pi_{\beta_{n-1}, \beta_n} = 0 \end{aligned} \quad (10c)$$

For Lamb wave with polarization [100; 010; 001],

$$\begin{aligned} & -\bar{u}_X \left[ \sum_{n=1}^N \bar{c}_{11}^{(n)} \pi_{\beta_{n-1}, \beta_n} + \bar{\sigma}_0^X \right] + \bar{u}'_X \sum_{n=1}^N \bar{c}_{55}^{(n)} \pi'_{\beta_{n-1}, \beta_n} + \bar{u}''_X \sum_{n=1}^N \bar{c}_{55}^{(n)} \pi_{\beta_{n-1}, \beta_n} + i\bar{u}_Z \sum_{n=1}^N \bar{c}_{55}^{(n)} \pi'_{\beta_{n-1}, \beta_n} \\ & - i\bar{u}'_Z \sum_{n=1}^N [\bar{c}_{55}^{(n)} + \bar{c}_{13}^{(n)}] \pi_{\beta_{n-1}, \beta_n} + i\bar{\phi} \sum_{n=1}^N \bar{e}_{15}^{(n)} \pi'_{\beta_{n-1}, \beta_n} + i\bar{\phi}' \sum_{n=1}^N [\bar{e}_{15}^{(n)} + \bar{e}_{31}^{(n)}] \pi_{\beta_{n-1}, \beta_n} = -\left(\frac{\Omega}{k}\right)^2 \bar{u}_X \sum_{n=1}^N \bar{\rho}^{(n)} \pi_{\beta_{n-1}, \beta_n} \end{aligned} \quad (11a)$$

$$\begin{aligned} & i\bar{u}_X \sum_{n=1}^N \bar{c}_{31}^{(n)} \pi'_{\beta_{n-1}, \beta_n} - i\bar{u}'_X \sum_{n=1}^N [\bar{c}_{55}^{(n)} + \bar{c}_{31}^{(n)}] \pi_{\beta_{n-1}, \beta_n} - \bar{u}_Z \left[ \sum_{n=1}^N \bar{c}_{55}^{(n)} \pi_{\beta_{n-1}, \beta_n} + \bar{\sigma}_0^X \right] + \bar{u}'_Z \sum_{n=1}^N \bar{c}_{33}^{(n)} \pi'_{\beta_{n-1}, \beta_n} + \bar{u}''_Z \sum_{n=1}^N \bar{c}_{33}^{(n)} \pi_{\beta_{n-1}, \beta_n} \\ & - \bar{\phi} \sum_{n=1}^N \bar{e}_{15}^{(n)} \pi_{\beta_{n-1}, \beta_n} + \bar{\phi}' \sum_{n=1}^N \bar{e}_{33}^{(n)} \pi'_{\beta_{n-1}, \beta_n} + \bar{\phi}'' \sum_{n=1}^N \bar{e}_{33}^{(n)} \pi_{\beta_{n-1}, \beta_n} = -\left(\frac{\Omega}{k}\right)^2 \bar{u}_Z \sum_{n=1}^N \bar{\rho}^{(n)} \pi_{\beta_{n-1}, \beta_n} \end{aligned} \quad (11b)$$

$$\begin{aligned} & i\bar{u}_X \sum_{n=1}^N \bar{e}_{31}^{(n)} \pi'_{\beta_{n-1}, \beta_n} + i\bar{u}'_X \sum_{n=1}^N [\bar{e}_{15}^{(n)} + \bar{e}_{31}^{(n)}] \pi_{\beta_{n-1}, \beta_n} - \bar{u}_Z \sum_{n=1}^N \bar{e}_{15}^{(n)} \pi_{\beta_{n-1}, \beta_n} + \bar{u}'_Z \sum_{n=1}^N \bar{e}_{33}^{(n)} \pi'_{\beta_{n-1}, \beta_n} + \bar{u}''_Z \sum_{n=1}^N \bar{e}_{33}^{(n)} \pi_{\beta_{n-1}, \beta_n} \\ & - \bar{\phi} \sum_{n=1}^N \bar{\varepsilon}_{11}^{(n)} \pi_{\beta_{n-1}, \beta_n} + \bar{\phi}' \sum_{n=1}^N \bar{\varepsilon}_{33}^{(n)} \pi'_{\beta_{n-1}, \beta_n} + \bar{\phi}'' \sum_{n=1}^N \bar{\varepsilon}_{33}^{(n)} \pi_{\beta_{n-1}, \beta_n} = 0 \end{aligned} \quad (11c)$$

In the above equations, the superscript prime is the partial derivative with respect to  $\beta$ , while the non-dimensional material constants are defined as  $\bar{c}_{ijkl}^{(n)} = \frac{c_{ijkl}^{(n)}}{c_{55}^{(1)}}$ ,  $\bar{e}_{kij}^{(n)} = \frac{e_{kij}^{(n)}}{\sqrt{c_{55}^{(1)} c_{33}^{(1)}}}$ ,  $\bar{\varepsilon}_{kj}^{(n)} = \frac{\varepsilon_{kj}^{(n)}}{c_{33}^{(1)}}$  and.

## 2.2. Legendre polynomial solutions

The above governing Eqs. (9)–(11) for SH and Lamb waves are solved using the Legendre polynomial method, since the Legendre polynomial has the merits of fast convergence and orthogonality. Then, the non-dimensional displacement  $\bar{u}_X(\beta)$ ,  $\bar{u}_Y(\beta)$ ,  $\bar{u}_Z(\beta)$  and electric potential  $\bar{\phi}(\beta)$  are further expanded into a series in terms of a set of orthogonal basis functions as follows,

$$\bar{u}_i(\beta) = \sum_{m=0}^{\infty} p_m^i Q_m(\beta), \quad \bar{\phi}(\beta) = \sum_{m=0}^{\infty} r_m Q_m(\beta) \quad (12)$$

where  $p_m^i$  ( $i=X, Y, Z$ ) and  $r_m$  are the expansion coefficients, and  $Q_m(\beta)$  is the set of polynomials orthonormal in the interval  $[0, kH]$  given by:

$$Q_m(\beta) = \sqrt{\frac{2m+1}{kH}} P_m(\tilde{\beta}) \quad (13)$$

where  $P_m(\tilde{\beta})$  is the  $m$ -th order Legendre polynomial with  $\tilde{\beta} = \frac{2\beta}{kH} - 1$ .

Substituting Eq. (12) into Eqs. (9)–(11) and multiplying the equations by the complex conjugate  $Q_j^*(\beta)$  with further integrating over  $\beta$  from 0 to  $kH$ . Taking advantage of orthonormality of the Legendre polynomials which is truncated at the  $M$ -th term gives the final characteristic equations for the wave propagation. For [010; 001; 100] SH waves,

$$\mathbf{A}_{22} \mathbf{p}^Y + \mathbf{A}_{24} \mathbf{r} = - \left( \frac{\Omega}{\bar{k}} \right)^2 \mathbf{M} \mathbf{p}^Y \quad (14a)$$

$$\mathbf{A}_{42} \mathbf{p}^Y - \mathbf{A}_{44} \mathbf{r} = \mathbf{0} \quad (14b)$$

For [001; 100; 010] and [100; 010; 001] Lamb waves,

$$\mathbf{A}_{11} \mathbf{p}^X + \mathbf{A}_{13} \mathbf{p}^Z + \mathbf{A}_{14} \mathbf{r} = - \left( \frac{\Omega}{\bar{k}} \right)^2 \mathbf{M} \mathbf{p}^X \quad (15a)$$

$$\mathbf{A}_{31} \mathbf{p}^X + \mathbf{A}_{33} \mathbf{p}^Z + \mathbf{A}_{34} \mathbf{r} = - \left( \frac{\Omega}{\bar{k}} \right)^2 \mathbf{M} \mathbf{p}^Z \quad (15b)$$

$$\mathbf{A}_{41} \mathbf{p}^X + \mathbf{A}_{43} \mathbf{p}^Z - \mathbf{A}_{44} \mathbf{r} = \mathbf{0} \quad (15c)$$

where  $\mathbf{p}^i = [p_0^i \quad p_1^i \quad \dots \quad p_M^i]^T$  and  $\mathbf{r} = [r_0 \quad r_1 \quad \dots \quad r_M]^T$ ,  $\mathbf{A}_{pq}$  and  $\mathbf{M}$  are the coefficient matrices with dimension  $(M+1) \times (M+1)$ . Note that the Lamb waves in [001; 100; 010] and [100; 010; 001] polarized composites hold the same form of characteristics Eq. (15), but the coefficient matrices  $\mathbf{A}_{pq}$  differ in their exact contents.

For either SH or Lamb waves, we may eliminate  $\mathbf{r}$  with the aid of Eqs. (14b) or (15c). Then the final characteristic equations for the guided wave propagation in the structure are reduced to an eigenequation as

$$(\mathbf{A}_{11} + \mathbf{A}_{14} \mathbf{A}_{44}^{-1} \mathbf{A}_{41}) \mathbf{p}^X + (\mathbf{A}_{13} + \mathbf{A}_{14} \mathbf{A}_{44}^{-1} \mathbf{A}_{43}) \mathbf{p}^Z = - \left( \frac{\Omega}{\bar{k}} \right)^2 \mathbf{M} \mathbf{p}^X \quad (16a)$$

$$\mathbf{A}_{22} \mathbf{p}^Y + \mathbf{A}_{24} \mathbf{A}_{44}^{-1} \mathbf{A}_{42} \mathbf{p}^Y = - \left( \frac{\Omega}{\bar{k}} \right)^2 \mathbf{M} \mathbf{p}^Y \quad (16b)$$

$$(\mathbf{A}_{31} + \mathbf{A}_{34} \mathbf{A}_{44}^{-1} \mathbf{A}_{41}) \mathbf{p}^X + (\mathbf{A}_{33} + \mathbf{A}_{34} \mathbf{A}_{44}^{-1} \mathbf{A}_{43}) \mathbf{p}^Z = - \left( \frac{\Omega}{\bar{k}} \right)^2 \mathbf{M} \mathbf{p}^Z \quad (16c)$$

Obviously, Eq. (16b) is independent of the other two and represents the propagation of SH waves in the structure, while Eq. (16a) and (c) controls the propagation of Lamb waves. The equations constitute a standard eigen-problem with the eigen-value  $\Omega/\bar{k} = V_{ph}/V_s$  which is the normalized phase velocity of the guided wave with  $V_{ph} = \omega/k$  denoting the phase velocity in the structure, while  $V_s = \sqrt{c_{55}^{(1)} / \rho^{(1)}}$  the shear wave velocity in the first layer. Note that the size of the characteristic Eq. (16)  $3(M+1)$  is defined by the truncated terms  $M$  of the Legendre polynomial expansion in Eq. (12), which also determines the convergence characteristics of the solution for guided wave propagation in the structure.

**Table 1**  
Properties of the piezoelectric PZT-4 plate [35].

Symbols parameter	PZT4
$\rho$ (kg/m <sup>3</sup> )	7500
$C_{ijkl}$ ( $\times 10^9$ N/m <sup>2</sup> )	$\begin{bmatrix} 139 & 78 & 74 & 0 & 0 & 0 \\ 78 & 139 & 74 & 0 & 0 & 0 \\ 74 & 74 & 115 & 0 & 0 & 0 \\ 0 & 0 & 0 & 25.6 & 0 & 0 \\ 0 & 0 & 0 & 0 & 25.6 & 0 \\ 0 & 0 & 0 & 0 & 0 & 30.5 \end{bmatrix}$
$e_{ij}$ (C/m <sup>2</sup> )	$\begin{bmatrix} 0 & 0 & 0 & 0 & 12.7 & 0 \\ 0 & 0 & 0 & 12.7 & 0 & 0 \\ -5.2 & -5.2 & 15.1 & 0 & 0 & 0 \end{bmatrix}$
$\varepsilon_{ij}$ ( $\times 10^{-9}$ C/Vm)	$\begin{bmatrix} 6.5 & 0 & 0 \\ 0 & 6.5 & 0 \\ 0 & 0 & 5.6 \end{bmatrix}$

**Table 2**  
Properties of the piezoelectric PZT-5A plate [36].

Symbols parameter	PZT-5A
$\rho$ (kg/m <sup>3</sup> )	7750
$C_{ijkl}$ ( $\times 10^9$ N/m <sup>2</sup> )	$\begin{bmatrix} 99.201 & 54.016 & 50.778 & 0 & 0 & 0 \\ 54.016 & 99.201 & 50.778 & 0 & 0 & 0 \\ 50.778 & 50.778 & 86.856 & 0 & 0 & 0 \\ 0 & 0 & 0 & 21.1 & 0 & 0 \\ 0 & 0 & 0 & 0 & 21.1 & 0 \\ 0 & 0 & 0 & 0 & 0 & 22.6 \end{bmatrix}$
(C/m <sup>2</sup> )	$\begin{bmatrix} 0 & 0 & 0 & 0 & 12.322 & 0 \\ 0 & 0 & 0 & 12.322 & 0 & 0 \\ -7.209 & -7.209 & 15.118 & 0 & 0 & 0 \end{bmatrix}$
( $\times 10^{-9}$ C/Vm)	$\begin{bmatrix} 1.53 & 0 & 0 \\ 0 & 1.53 & 0 \\ 0 & 0 & 1.5 \end{bmatrix}$

### 3. Numerical results and discussions

As mentioned previously, the presence of initial mechanical stress in the multilayer plates is often inevitable due to chemical shrinkage, material growth, enhancing fracture toughness, mismatching thermal expansion, machining at different temperature, and creep deformation, etc. This initial mechanical stress for the PZT-4/PZT-5A composites might lead to the dramatically change in characteristics of guided waves. Based on the above outlined formulations, we calculate numerically the effect of initial stress on the characteristics of guided waves in piezoelectric multilayer composite systems based on Matlab program codes. The material properties of PZT-4 and PZT-5A are given in Tables 1 [35] and 2 [36], respectively. This part mainly focuses on the convergence property and accuracy validation of the polynomial method and the effects of initial stresses on the SH and Lamb waves. It should be noted that the initial mechanical stress, mechanical field, and electric field cannot be independent, as they must be self-consistent. Consequently, the self-consistent condition of the initial biasing field should be satisfied, which indicates that the assumed initial stress components  $\sigma_X^0$  should be self-balanced by an electric field  $D_Z^0 = \sigma_X^0(c_{13}e_{33} - c_{33}e_{31})/(c_{13}^2 - c_{11}c_{33})$  in the open circuit case.

To evaluate the convergence of the Legendre polynomial method for the guided SH and Lamb waves, different values of the truncated term number  $M$  are taken to calculate the dispersion curves of the SH waves (Fig. 2a) and Lamb waves (Fig. 2b and c) in a layered PZT-4/PZT-5A/PZT-4 system without initial stresses ( $\sigma_X^0 = 0$ ). It demonstrates that a truncated number  $M=10$  may yield converged results of the fundamental frequencies (mode with subscript 0) for various wave numbers. For higher modes, more truncated term number (e.g.,  $M=15$ ) is necessary to yield results with satisfying convergence which deviate slightly from those obtained using  $M=20$ . For the dimensionless phase velocity that has been injected in Fig. 2, our attempts for order truncation  $M=20$  (or higher than  $M=20$ ) showed that the velocity convergence is not completely reached for some modes by comparing with those obtained by exact ODE method [25] (Fig. 2(a) and (b)). Even so, this validates the Legendre polynomial method for phase velocities calculations and the convergence, but with such discrepancies which are strongly acceptable [27]. These discrepancies may be attributed to the approximation for the open-circuit boundary condition [27] and the low contrast between successive layers [27] as well using the Legendre polynomial method. It should be noted that this contrast level between the successive layers is widely developed by this polynomial method [29].

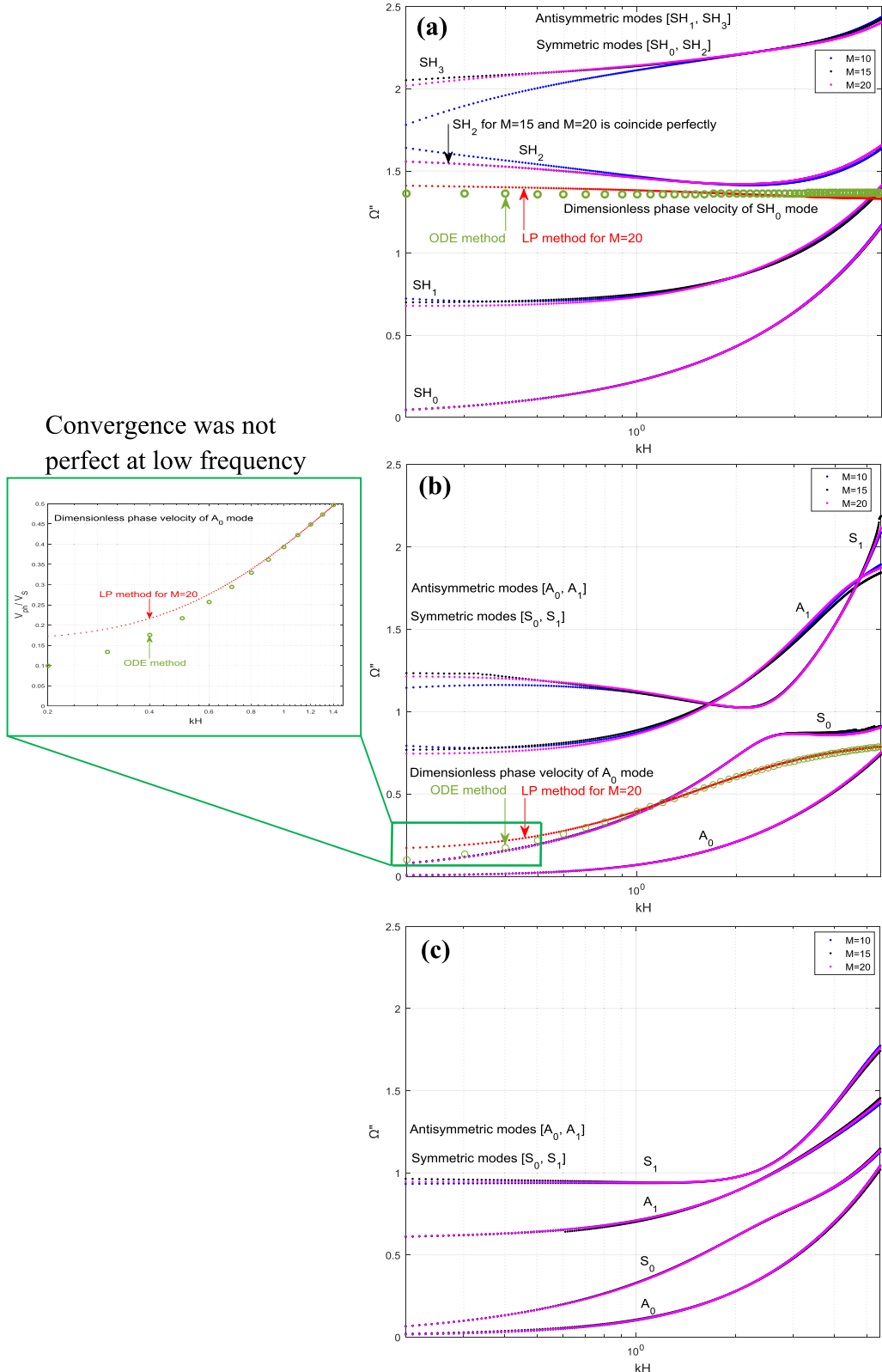


**Fig. 2.** Frequency spectrum of guided wave propagation in B/A/B piezoelectric sandwich structure according to expansion order  $M=10, 15$  and  $20$ : (a) [010;001;100] Shear horizontal (SH) waves; (b) [001;100;010] Lamb waves; (c) [100;010;001] Lamb waves.

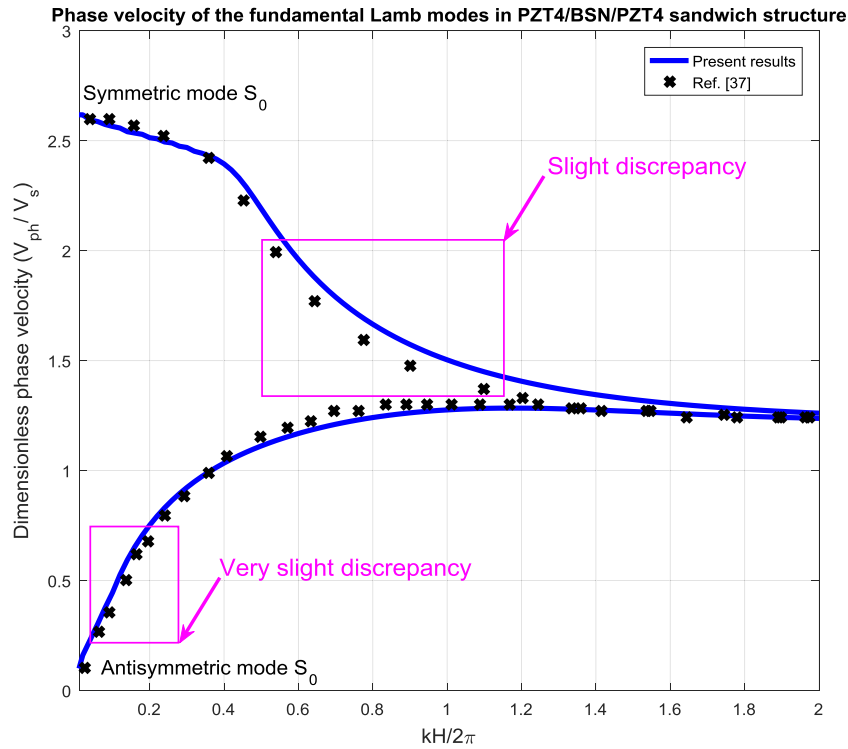


**Fig. 3.** Phase velocity of the fundamental Lamb modes in PZT4/BSN/PZT4 piezoelectric sandwich structure; (×) the results from the reverberation-ray matrix method [37]; (solid line) the results from the present Legendre polynomial method.

Hence, the series expansions in Eq. (12) are truncated at  $M=20$  for all calculations in following text. Here, the dimensionless frequency is defined as  $\Omega''=\frac{\omega H}{2\pi}\sqrt{\frac{\rho^{(1)}}{c_{55}^{(1)}}}$ .

To check the validity and the efficiency of our approach, we make a comparison between our results and the available data [37] for fundamental Lamb modes of a PZT-4/BSN/PZT-4 sandwich structure with open circuit. Fig. 3 presents the variation of normalized phase velocity  $V_{ph}/V_s$  versus the wave number  $kH/2\pi$  for the Lamb wave obtained using the present polynomial method and the reverberation-ray matrix method [37]. In general, excellent agreement between two methods solidly validates the accuracy of the present polynomial method. As mentioned above, the slight discrepancy in the fundamental symmetric Lamb mode may be attributed to the approximation for the open-circuit boundary condition and the low contrast between successive layers as well using the Legendre polynomial method.

To examine the influences of the initial stress  $\sigma_X^0$  on the guided wave propagation behaviors, the guided dispersion curves with different values of the initial stress are presented in Fig. 4. Here, the [010; 001; 100] SH waves, [001; 100; 010] Lamb waves and [100; 010; 001] Lamb waves have been retained to illustrate the initial stress effect. The Lamb waves can be divided into two family modes, the symmetric ( $S_m$ ) and anti-symmetric ( $A_m$ ) modes. In fact, the first and second fundamental Lamb modes in Fig. 4(c) and (e) is closely linked to the anti-symmetric ( $A_0$ ) and symmetric ( $S_0$ ), respectively. The two modes dominate over most of the frequency range in this type of three layers system. Consequently, the zero-order Lamb modes  $S_0$  and  $A_0$  are the only modes propagating when  $kH \rightarrow 0$ , which indicates these fundamental modes do not have a cut-off frequency. In addition, the phase velocity of  $S_0$  mode is constant at the neighborhood of  $kH=2$ , taking the value  $V_{ph}/V_s \approx 2.25$  and  $V_{ph}/V_s \approx 2.0$  for the [001; 100; 010] and [100; 010; 001] waves, respectively. Therefore, the  $S_0$  mode presents a non-dispersive tray in the low dimensionless wave number area (Fig. 4c and e). Moreover, the  $A_0$  mode is dispersive and its phase velocity in the low dimensionless wave number area is proportional to the square root of  $H$ .

For each polarization direction, the results without initial stress  $\sigma_X^0 = 0$ , with tensile stress  $\sigma_X^0 > 0$  [38] and with compressive stress  $\sigma_X^0 < 0$  [38] are shown in one figure to facilitate the comparison. It can be observed from Fig. 4(a), (c) and (e) that the influence of the both tensile and compressive stresses on guided dispersion curves becomes very significant, especially on the fundamental modes. This is further observed in Fig. 4(b), (d) and (f) where the relative increment of phase velocity is defined as  $\frac{\Delta V_{ph}}{V_{ph,0}} = \frac{V_{ph,\text{stress}} - V_{ph,0}}{V_{ph,0}} \times 100\%$  with  $V_{ph,\text{stress}}$  and  $V_{ph,0}$  denoting the phase velocity with and without initial stress. The increment of phase velocity increases with  $KH$  in a general manner except for the  $A_0$  whose increment decreases (Fig. 4d and f) while for SH<sub>0</sub> wave with  $\sigma_X^0 = 1$  GPa no significant increasing is observed (Fig. 4b). In addition, the higher level of initial stress, the more significant increasing in the phase velocity is achieved. From Fig. 4(a), (c) and (e) it

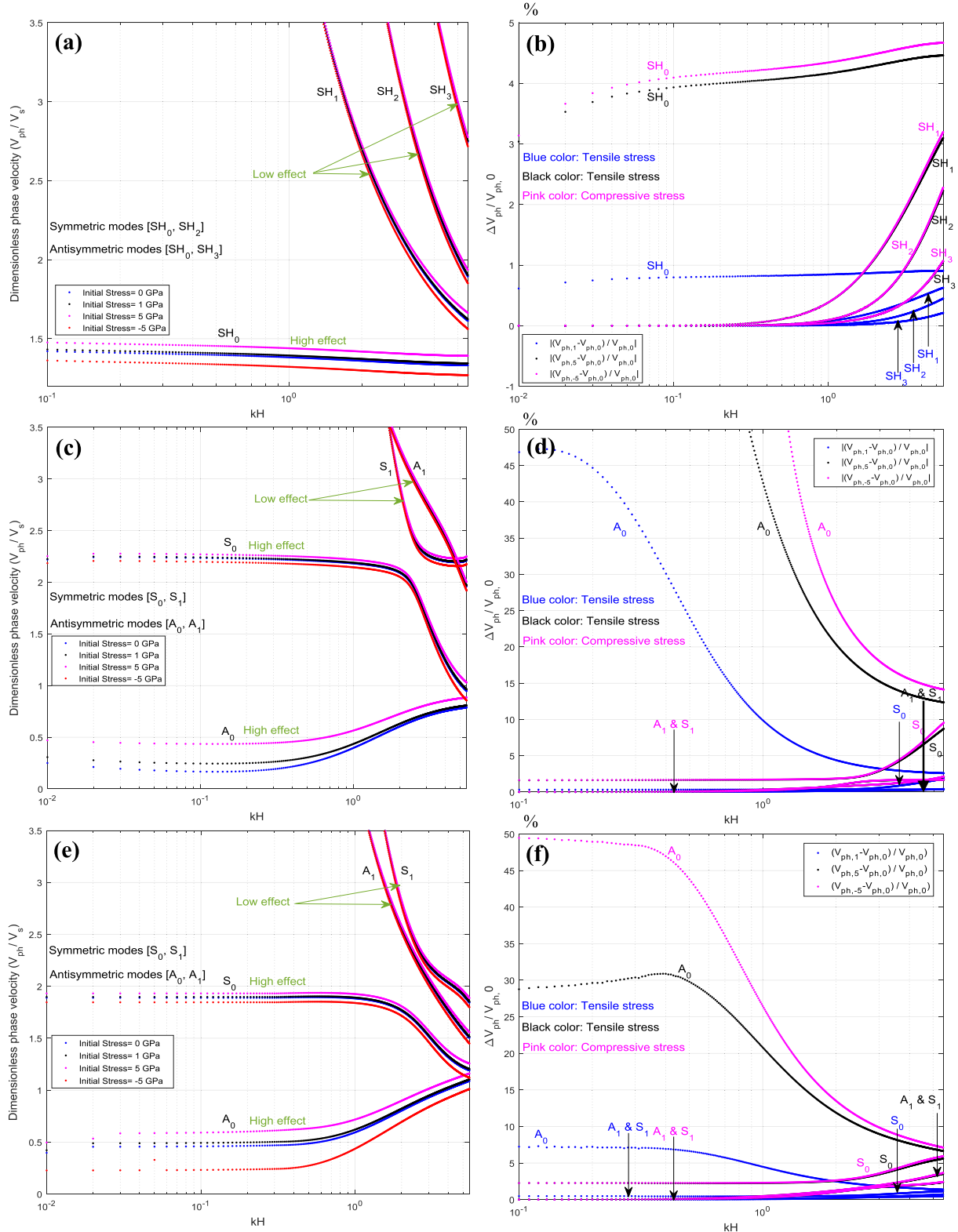


**Fig. 4.** Influence of initial stress on the guided dispersion curves in B/A/B piezoelectric sandwich structure for  $M=20$ : (a), [010;001;100] SH waves; (b), relative increment of phase velocity in Fig. 4(a); (c), [001;100;010] Lamb waves; (d), relative increment of phase velocity in Fig. 4(c); (e), [100;010;001] Lamb waves; (f), relative increment of phase velocity in Fig. 4(e).

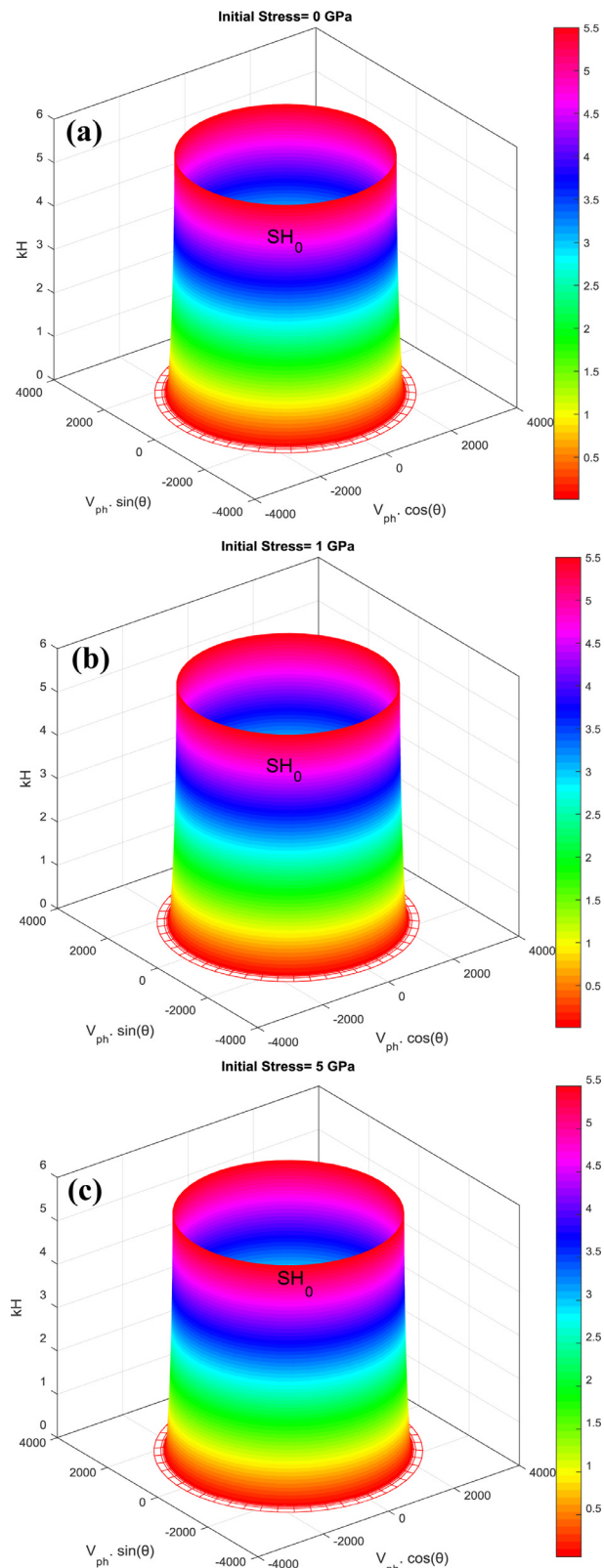


**Fig. 5.** 3D-view of fundamental  $\text{SH}_0$  mode for different initial stress in the B/A/B sandwich structure: (a) Initial Stress = 0 GPa; (b) Initial Stress = 1 GPa; (c) Initial Stress = 5 GPa.

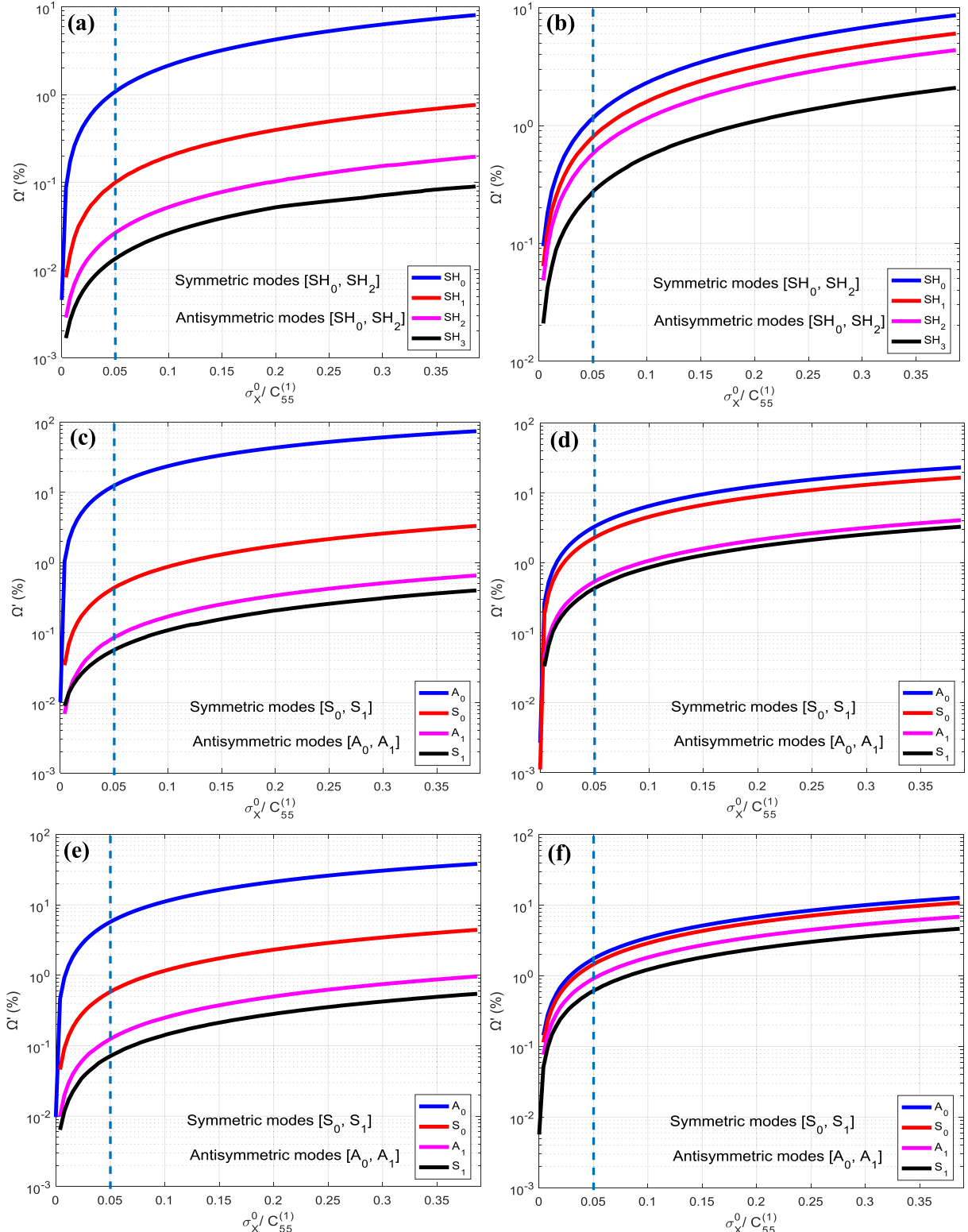


**Fig. 6.** Frequency spectrum  $\Omega'$  versus the dimensionless (initial stress/ $C_{55}$ ) for different values of  $kh$ : (a), [010;001;100] SH waves for  $kh = 1$ ; (b), [010;001;100] SH waves for  $kh = 5.5$ ; (c), [001;100;010] Lamb waves for  $kh = 1$ ; (d), [001;100;010] Lamb waves for  $kh = 5.5$ ; (e), [100;010;001] Lamb waves for  $kh = 1$ ; (f), [100;010;001] Lamb waves for  $kh = 5.5$ .

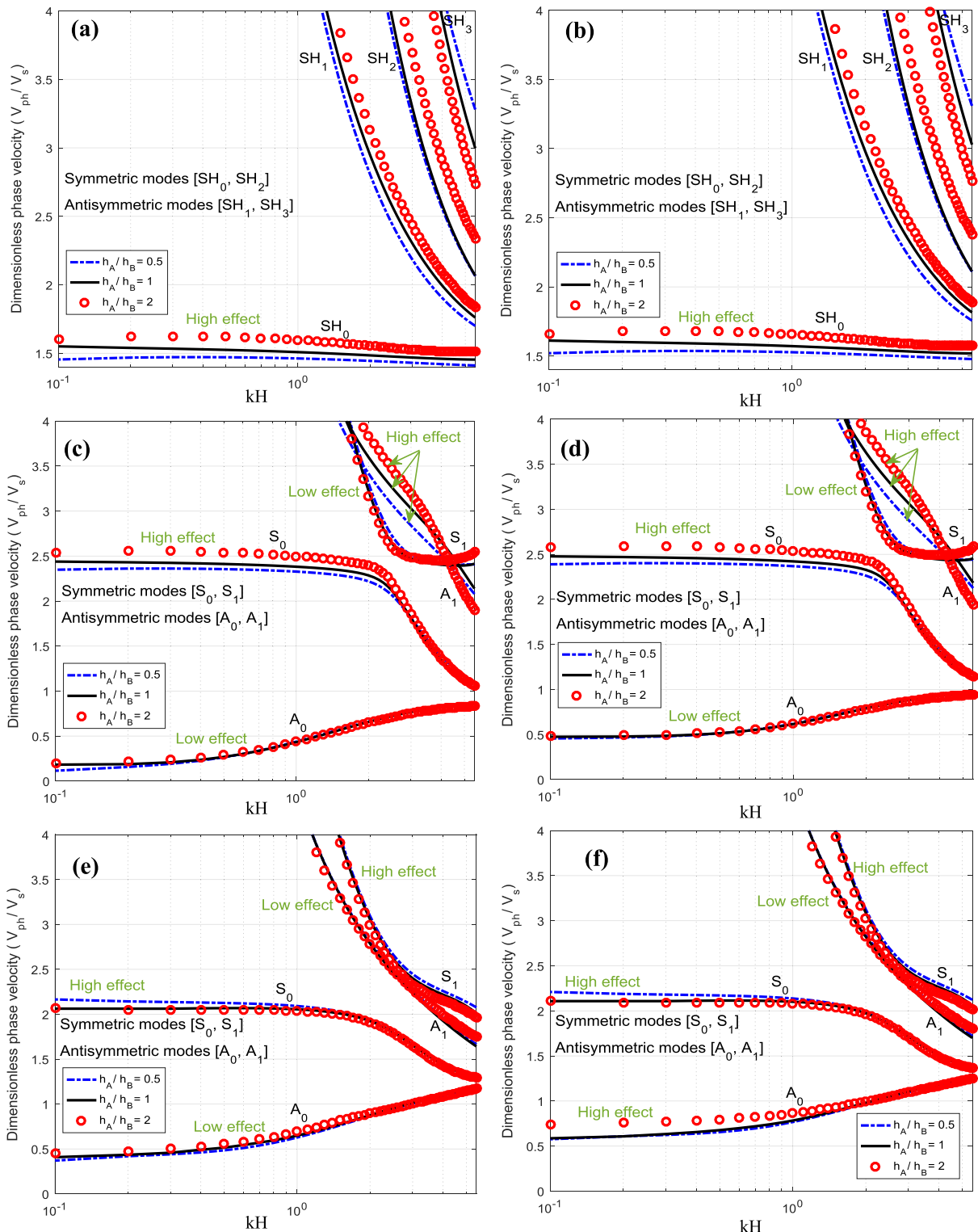


**Fig. 7.** Guided dispersion curves in B/A/B structure with varying the thickness of layers: (a), [010;001;100] SH waves for initial stress=0 GPa; (b), [010;001;100] SH waves for initial stress=5 GPa; (c), [001;100;010] Lamb waves for initial stress=0 GPa; (d), [001;100;010] Lamb waves for initial stress=5 GPa; (e), [100;010;001] Lamb waves for initial stress=0 GPa; (f), [100;010;001] Lamb waves for initial stress=5 GPa.

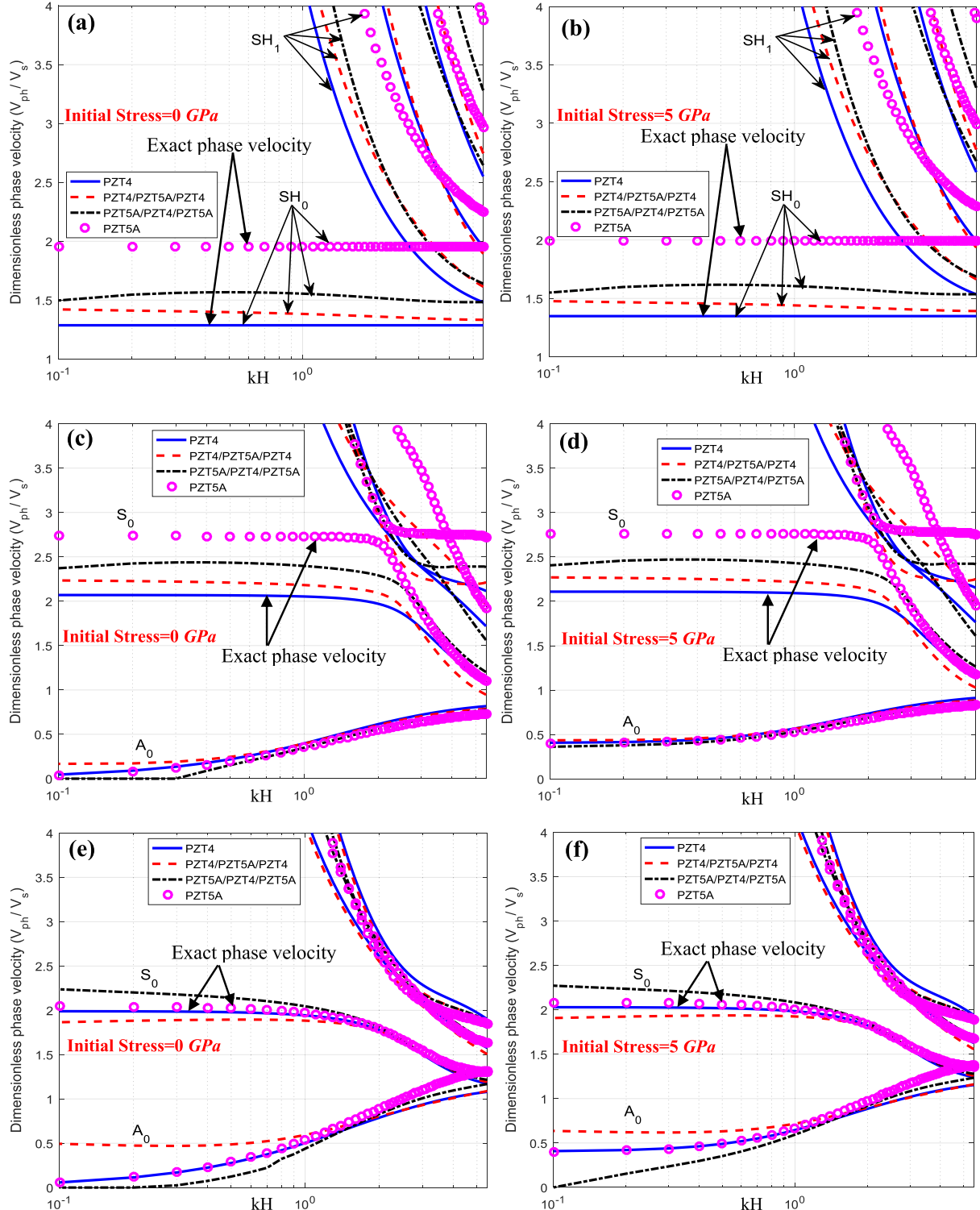


**Fig. 8.** Guided dispersion curves for different systems: (a), [010;001;100] SH waves for initial stress=0 GPa; (b), [010;001;100] SH waves for initial stress = 5 GPa; (c), [001;100;010] Lamb waves for initial stress = 0 GPa; (d), [001;100;010] Lamb waves for initial stress = 5 GPa; (e), [100;010;001] Lamb waves for initial stress = 0 GPa; (f), [100;010;001] Lamb waves for initial stress = 5 GPa.

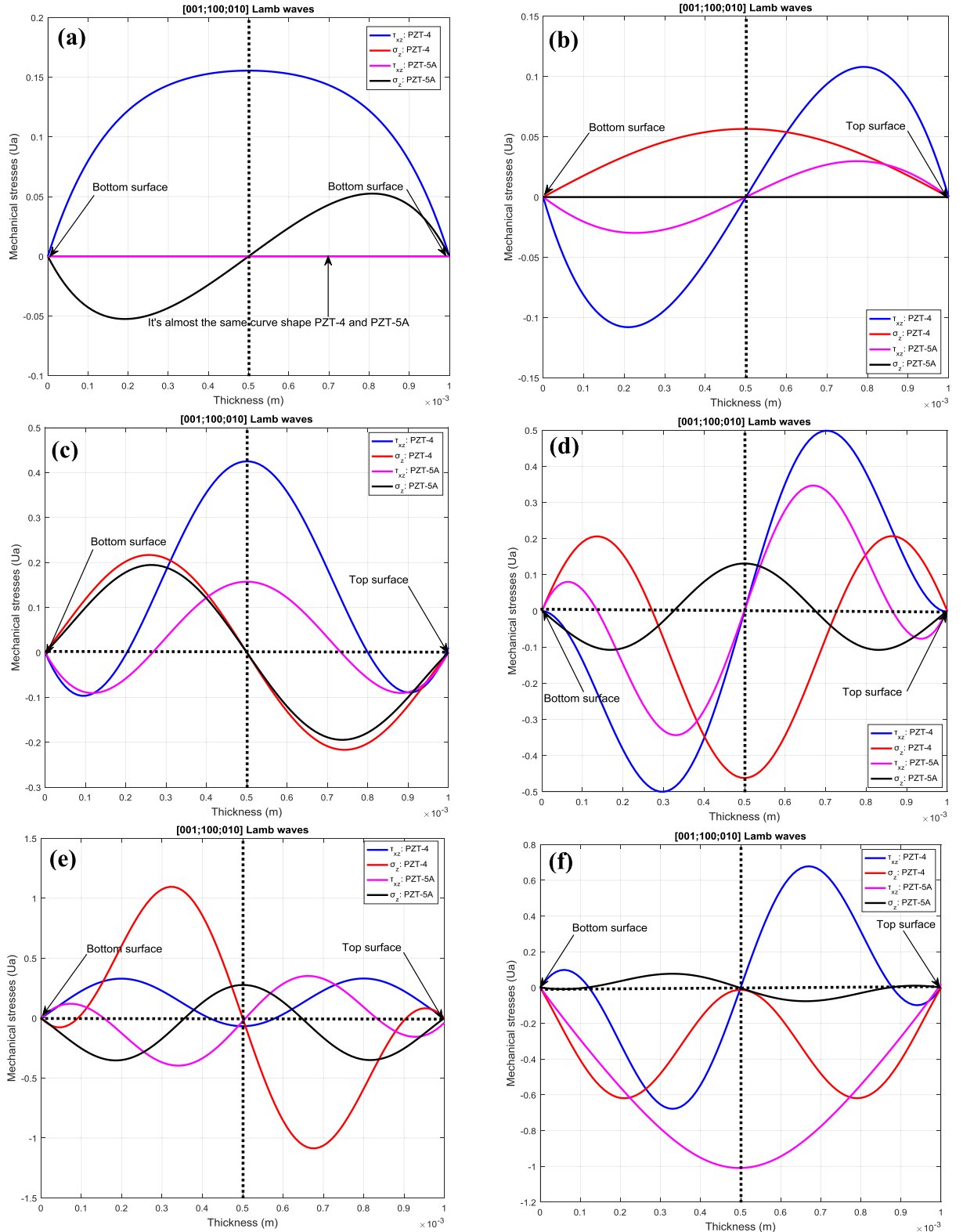


**Fig. 9.** Mechanical stresses of the first six Lamb modes in PZT-4 and PZT-5H piezoelectric plates: (a),  $A_0$  for  $kH = 5.5$ ,  $V_{PZT-4} = 1648.5 \text{ m/s}$ ,  $V_{PZT-5A} = 1470.5 \text{ m/s}$ ; (b),  $S_0$  for  $kH = 5.5$ ,  $V_{PZT-4} = 2243.2 \text{ m/s}$ ,  $V_{PZT-5A} = 2222 \text{ m/s}$ ; (c),  $A_1$  for  $kH = 5.5$ ,  $V_{PZT-4} = 3466 \text{ m/s}$ ,  $V_{PZT-5A} = 3863.3 \text{ m/s}$ ; (d),  $S_1$  for  $kH = 5.5$ ,  $V_{PZT-4} = 4266.5 \text{ m/s}$ ,  $V_{PZT-5A} = 5478.8 \text{ m/s}$ ; (e),  $A_2$  for  $kH = 5.5$ ,  $V_{PZT-4} = 4963.2 \text{ m/s}$ ,  $V_{PZT-5A} = 5729.3 \text{ m/s}$ ; (f),  $S_2$  for  $kH = 5.5$ ,  $V_{PZT-4} = 5018.4 \text{ m/s}$ ,  $V_{PZT-5A} = 6188.5 \text{ m/s}$ .

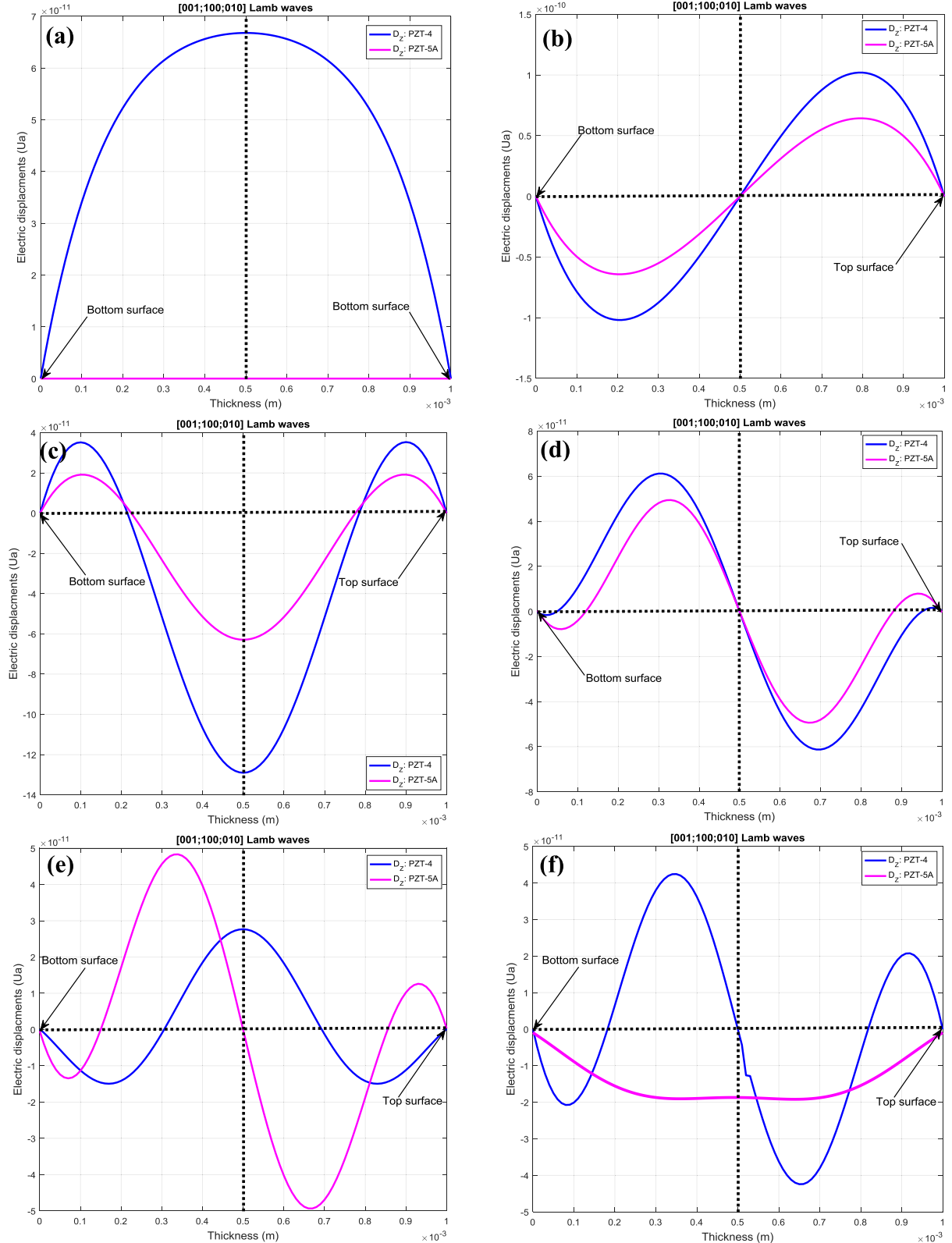


**Fig. 10.** Electric displacements of the first six Lamb modes in PZT-4 and PZT-5H piezoelectric plates: (a),  $A_0$  for  $kH=5.5$ ,  $V_{PZT-4}=1648.5 \text{ m/s}$ ,  $V_{PZT-5A}=1470.5 \text{ m/s}$ ; (b),  $S_0$  for  $kH=5.5$ ,  $V_{PZT-4}=2243.2 \text{ m/s}$ ,  $V_{PZT-5A}=2222 \text{ m/s}$ ; (c),  $A_1$  for  $kH=5.5$ ,  $V_{PZT-4}=3466 \text{ m/s}$ ,  $V_{PZT-5A}=3863.3 \text{ m/s}$ ; (d),  $S_1$  for  $kH=5.5$ ,  $V_{PZT-4}=4266.5 \text{ m/s}$ ,  $V_{PZT-5A}=5478.8 \text{ m/s}$ ; (e),  $A_2$  for  $kH=5.5$ ,  $V_{PZT-4}=4963.2 \text{ m/s}$ ,  $V_{PZT-5A}=5729.3 \text{ m/s}$ ; (f),  $S_2$  for  $kH=5.5$ ,  $V_{PZT-4}=5018.4 \text{ m/s}$ ,  $V_{PZT-5A}=6188.5 \text{ m/s}$ .

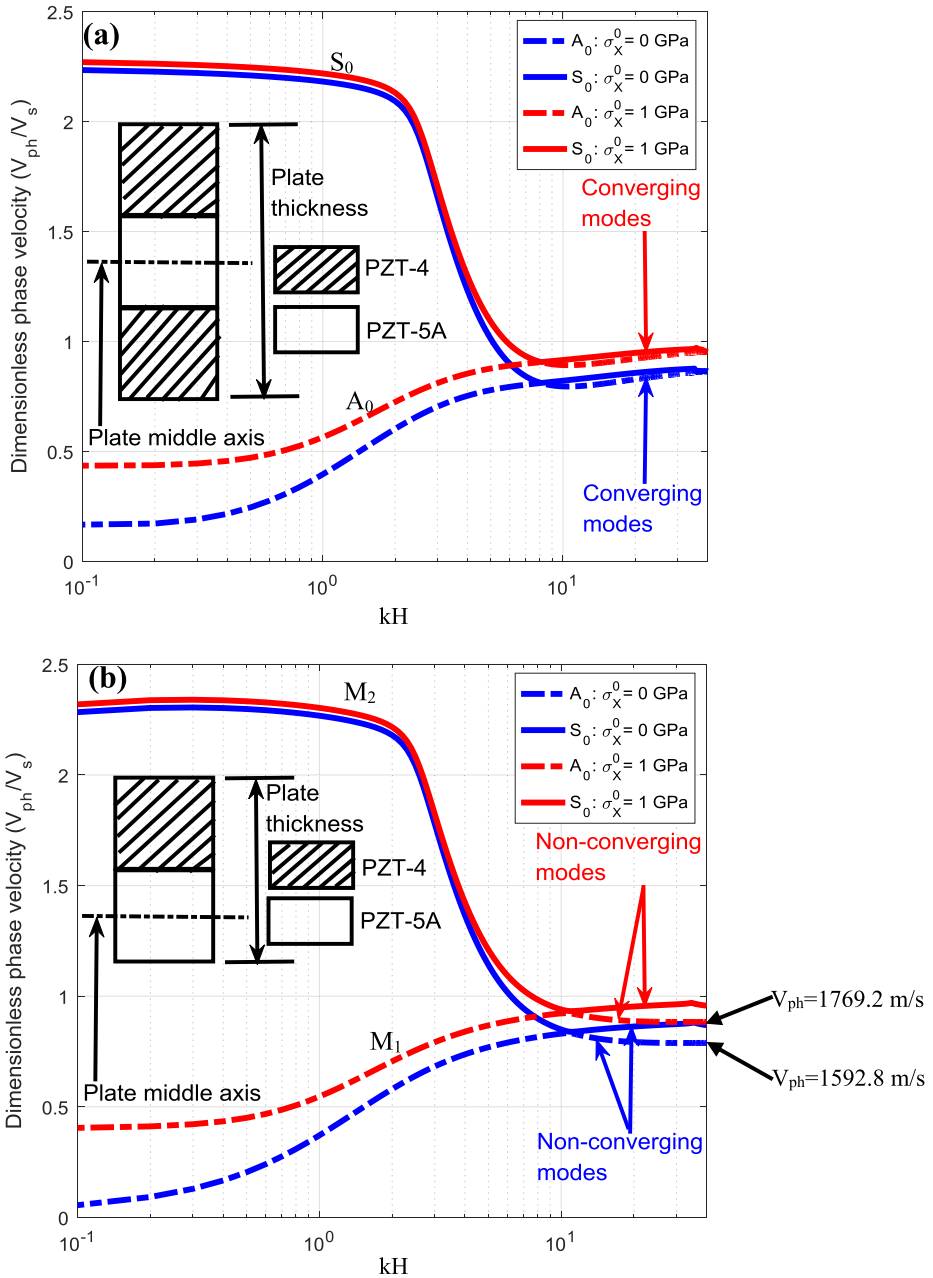


**Fig. 11.** Fundamental [001;100;010] Lamb modes with different initial stress values: (a) Symmetrical plate configuration; (b) Unsymmetrical plate configuration.

can be seen that the influences of the initial stress on the dispersion relations are different for the compression stress case and the tensile stress case. Accordingly, we may conclude that the positive initial stresses make the phase velocity of Lamb and SH waves increasing, while the negative initial stresses make it decreasing. In addition, this kind of increase (tensile stress) or decrease (compressive stress) in phase velocity for lower modes is much significant than higher modes. This is potentially attributed to the presence of initial stress that brings the constituent particles closer to each other and thus leads towards more compact and denser medium which encourages the Lamb and SH phase velocity [39]. On the other hand, it is clear from Fig. 4(a), (c) and (e) that the polarization direction has great influence on the Lamb dispersion curves for the various initial stress values. As expected, the open-circuit guided phase velocity is retrieved with an acceptable discrepancy. This discrepancy is attributed to the use of the approximate open-circuit boundary conditions [27] and the low contrast of PZT4-PZT5A multilayered structures [27] as well. Another important thing to note is that in contrast to the propagation

feature of SH waves in elastic plates, the zero-order SH wave is lightly dispersive for piezoelectric structures (Fig. 5) for various initial stresses. This phenomenon is no doubt induced by the electromechanical coupling effects of piezoelectric materials. Fig. 5 is represented in a three-dimensional Cartesian coordinate system ( $X$ ,  $Y$ ,  $Z$ ), with  $Z$  is the axis of  $kH$ :  $Z=kH$ ; and  $(X, Y)$  are the phase velocity whose  $X=V_{ph} \cdot \cos(\theta)$  and  $Y=V_{ph} \cdot \sin(\theta)$ . Here,  $\theta$  range from 0 to  $2\pi$ .

Fig. 6 presents the variation of the relative frequency change  $\Omega' = \frac{\Omega_{\text{with}} - \Omega_{\text{without}}}{\Omega_{\text{without}}} \times 100\%$  for SH and Lamb waves for  $kH=1$  and  $kH=5.5$ , where the subscript 'with' and 'without' indicate the case including and excluding the effects of initial stress. The frequency increment increases with the initial stress and smaller wave length (Fig. 6a, c, and e) may induce more significant relative increment in the frequency than larger wave length (Fig. 6b, d, and f). Effects of the thickness of PZT-4 and PZT-5A on the wave propagation characteristics of the PZT-4/PZT-5A/PZT-4 composites are analyzed in Fig. 7 with  $H_A$  and  $H_B$ , respectively representing the thickness of the PZT-5A and PZT-4. Whether considering the effects of initial stress or not, the thickness of the component layer poses significant influences on the wave propagation of both SH and Lamb waves. However, these guided modes always converge to a same limit case.

Keeping the entire thickness of the plate constant and change the composition layer, the wave propagation properties will be manipulated significantly (Fig. 8). Due to the significant differences in elastic, piezoelectric and dielectric properties between PZT-4 and PZT-5A, the dispersion curves behaviors of these plates with various components differ from each other evidently. For the majority of Lamb and SH modes, the phase velocity in a three-layered PZT-4 and PZT-5A composite plates locate between those of the pure PZT-4 and PZT-5A piezoelectric homogeneous plates (Fig. 8). In general, PZT-5A provides a higher phase velocity than PZT-4, thus making the fact that the PZT-4/PZT-5A/PZT-4 composites exhibits lower phase velocity than the PZT-5A/PZT-4/PZT-5A. This is obviously caused by the volume fraction of these two materials. In this context, we shall consider the mode shapes of the mechanical stresses and electric displacement of the Lamb waves in PZT-4 and PZT-5A piezoelectric homogeneous plates. The goal here is to check the stability of our polynomial method to apply the different mechanical and electrical boundary conditions. The electrically open condition at the surface is considered and initial stress  $\sigma_X^0 = 0$  with  $kH=5.5$ . The results are correspondingly shown in Figs. 9 and 10. For the both structures, it can be seen that the mechanical stresses  $\tau_{XZ}$ ,  $\sigma_Z$  and electric displacement  $D_Z$  for the first six Lamb modes are zero on the top and bottom surfaces. It should be noted that the electrical boundary conditions used in this work is approximate ( $D_Z \pi_{0,kh}(\beta)$ ). Consequently, the electric displacement  $D_Z$  is assumed to be zero rather than continuous, that's mean the electric displacement of the vacuum is neglected [5–7]. These results well meets well ours with the different boundary conditions applied and agreement with the free character of the lower and upper surfaces of the structure. Furthermore, it can be concluded that the piezoelectric material kind have considerable effect on the mechanical stresses and electric displacement distributions for the Lamb modes shapes.

The comparison between unsymmetrical and symmetrical structures for different initial stress values is shown in Fig. 11. The symmetric structure is composed of three piezoelectric layers, the fundamental  $S_0$  and  $A_0$  modes converge and stay joined at a lower  $kH$  (Fig. 9a) compared with the quasi- $S_0$  and quasi- $A_0$  modes in the unsymmetrical piezoelectric plate (Fig. 9b). In the symmetric configuration, the modes, like purely homogeneous plate, are anti-symmetric and symmetric and can be denoted by  $A_n$  and  $S_n$  ( $n=0, 1, 2, 3..$ ), while, for the unsymmetrical configuration, the feature of symmetry and anti-symmetry in wave modes is not obvious [31]. From Fig. 11b, we also observe that the  $A_0$  phase velocity for the bilayer structure for high  $kH$  values tends asymptotically toward  $V_{ph}=1592.8$  m/s which corresponds to the  $A_0$  and  $S_0$  phase velocities in homogeneous PZT-5A. For the symmetric Lamb modes  $S_0$ , when  $kH$  becomes large, the phase velocity tends asymptotically toward  $V_{ph}=1769.2$  m/s which corresponds to the  $A_0$  and  $S_0$  phase velocities in homogeneous PZT-4.

#### 4. Conclusions

The influences of initial stress on guided wave behaviors in multilayered PZT-4/PZT-5A composites were investigated based on a three-dimensional analysis. Using the Legendre polynomial approach, the characteristic equations governing the dispersion relations for the composites were derived in purely algebraic forms. Numerical results compared very well with those reported in literature, thus validating the current solutions. It was also established that the polynomial approach exhibits high stability and fast convergence for the current multilayered piezoelectric structures. Theoretical calculations demonstrate that initial stresses may pose significant influences on the Lamb and SH waves behaviors in piezoelectric multilayer composites. Phase velocities of Lamb and SH waves increases with the initial tensile stress, which is regarded as increasing the rigidity of the structure. It suggests that the effects of initial stress of  $\sigma_X^0/c_{55}^{(1)} > 0.05$  on the frequency spectrum is significant while that in the range of  $\sigma_X^0/c_{55}^{(1)} < 0.05$  is indistinguishable. Furthermore, the effects of polarization direction, thickness and stacking sequences of constituent piezoelectric layers on the guided wave characteristics were also investigated.

#### Acknowledgments

This work was supported by the National Natural Science Foundation of China through Grant nos. 11621062 and 11772295, and was also partly supported by the Fundamental Research Funds for the Central Universities 2016XZZX001-05. The authors would like to thank the anonymous reviewers for their valuable comments.

## Appendix A

The relationships of  $C_{ijkl}$  and  $C_{ij}$  are:

$$C_{ijkl} : \begin{bmatrix} C_{1111} & C_{1122} & C_{1133} & C_{1123} & C_{1131} & C_{1112} \\ C_{2211} & C_{2222} & C_{2233} & C_{2223} & C_{2231} & C_{2212} \\ C_{3311} & C_{3322} & C_{3333} & C_{3323} & C_{3331} & C_{3312} \\ C_{2311} & C_{2322} & C_{2333} & C_{2323} & C_{2331} & C_{2312} \\ C_{3111} & C_{3122} & C_{3133} & C_{3123} & C_{3131} & C_{3112} \\ C_{1211} & C_{1222} & C_{1233} & C_{1223} & C_{1231} & C_{1212} \end{bmatrix} = c_{ij} : \begin{bmatrix} C_{11} & C_{12} & C_{13} & 0 & 0 & 0 \\ C_{21} & C_{22} & C_{23} & 0 & 0 & 0 \\ C_{31} & C_{32} & C_{33} & 0 & 0 & 0 \\ 0 & 0 & 0 & C_{44} & 0 & 0 \\ 0 & 0 & 0 & 0 & C_{55} & 0 \\ 0 & 0 & 0 & 0 & 0 & C_{66} \end{bmatrix}$$

The relationships of  $e_{ijk}$  and  $e_{ij}$  are:

- Polarization [0 1 0; 0 1; 1 0 0],

$$e_{ijk} : \begin{bmatrix} e_{111} & e_{122} & e_{133} & e_{123} & e_{131} & e_{112} \\ e_{211} & e_{222} & e_{233} & e_{223} & e_{231} & e_{212} \\ e_{311} & e_{322} & e_{333} & e_{323} & e_{331} & e_{312} \end{bmatrix} = e_{ij} : \begin{bmatrix} 0 & 0 & 0 & 0 & 0 & e_{16} \\ e_{21} & e_{22} & e_{23} & 0 & 0 & 0 \\ 0 & 0 & 0 & e_{34} & 0 & 0 \end{bmatrix}$$

- Polarization [1 0 0; 0 1 0; 0 0 1],

$$e_{ijk} : \begin{bmatrix} e_{111} & e_{122} & e_{133} & e_{123} & e_{131} & e_{112} \\ e_{211} & e_{222} & e_{233} & e_{223} & e_{231} & e_{212} \\ e_{311} & e_{322} & e_{333} & e_{323} & e_{331} & e_{312} \end{bmatrix} = e_{ij} : \begin{bmatrix} 0 & 0 & 0 & 0 & e_{15} & 0 \\ 0 & 0 & 0 & e_{24} & 0 & 0 \\ e_{31} & e_{32} & e_{33} & 0 & 0 & 0 \end{bmatrix}$$

- Polarization [0 0 1; 1 0 0; 0 1 0],

$$e_{ijk} : \begin{bmatrix} e_{111} & e_{122} & e_{133} & e_{123} & e_{131} & e_{112} \\ e_{211} & e_{222} & e_{233} & e_{223} & e_{231} & e_{212} \\ e_{311} & e_{322} & e_{333} & e_{323} & e_{331} & e_{312} \end{bmatrix} = e_{ij} : \begin{bmatrix} e_{31} & e_{32} & e_{33} & 0 & 0 & 0 \\ 0 & 0 & 0 & 0 & 0 & e_{26} \\ 0 & 0 & 0 & e_{35} & 0 & 0 \end{bmatrix}$$

## References

- [1] J. Curie, P. Curie, Bulletin de la Société minéralogique de France, 4, 1880; 90–93.
- [2] J. Sun, Z. Wang, Z. Zhou, X. Xu, C.W. Lim, Surface effects on the buckling behaviors of piezoelectric cylindrical nanoshells using nonlocal continuum model, *Appl. Math. Model.* 59 (2018) 341–356.
- [3] Y.Y. Zhou, W.Q. Chen, C.F. Lü, Semi-analytical solution for orthotropic piezoelectric laminates in cylindrical bending with interfacial imperfections, *Compos. Struct.* 92 (2010) 1009–1018.
- [4] Y. Wei, J. Wang, W.Q. Chen, Cylindrical bending responses of angle-ply piezoelectric laminates with viscoelastic interfaces, *Appl. Math. Model.* 38 (2014) 6018–6030.
- [5] C. Othmani, F. Takali, A. Njeh, Legendre polynomial modeling for vibrations of guided Lamb waves modes in [001]c, [011]c and [111]c polarized (1-x)P(Mg1/3Nb2/3)O3-xPbTiO3 (x=0.29 and 0.33) piezoelectric plates: physical phenomenon of multiple intertwining of  $A_n$  and  $S_n$  modes, *Eur. Phys. J. Plus* 132 (2017) 1–19.
- [6] C. Othmani, F. Takali, A. Njeh, Investigating and modeling of effect of piezoelectric material parameters on shear horizontal (SH) waves propagation in PZT-5H, PMN-0.33pt and PMN-0.29pt plates, *Optik* 148 (2017) 63–75.
- [7] C. Othmani, F. Takali, A. Njeh, Theoretical study on the dispersion curves of Lamb waves in piezoelectric semiconductor sandwich plates GaAs-FGP-M-AlAs: legendre polynomial series expansion, *Superlattices Microstruct.* 106 (2017) 86–101.
- [8] A.H. Nayfeh, *Wave Propagation in Layered Anisotropic Media*, Elsevier, North Holland, Amsterdam, 1995.
- [9] B.A. Auld, *Acoustic Fields and Waves in Solids*, Krieger, Malabar, FL, 1990.
- [10] R.W. Ogden, Incremental elastic motions superimposed on a finite deformation in the presence of an electromagnetic field, *Int. J. Nonlinear Mech.* 44 (2009) 570–580.
- [11] P. Saxena, R.W. Ogden, On surface waves in a finitely deformed magnetoelastic half-space, *Int. J. Appl. Mech.* 3 (2011) 633–665.
- [12] P. Saxena, R.W. Ogden, On Love-type waves in a finitely deformed magnetoelastic layered half-space, *Zeitschrift für Angewandte Mathematik und Physik* 63 (2012) 1177–1200.
- [13] Y.Y. Zhou, C.F. Lü, W.Q. Chen, Bulk wave propagation in layered piezomagnetic/piezoelectric plates with initial stresses or interface imperfections, *Compos. Struct.* 94 (2012) 2736–2745.
- [14] L. Jie, Z. Jinxiang, Propagation of Lamb waves in a pre-stressed plate, *Appl. Mech. Mater.* 66 (2011) 413–441.
- [15] M.S. Son, Y.J. Kang, The effect of initial stress on the propagation behavior of SH waves in piezoelectric coupled plates, *Ultrasonics* 51 (2011) 489–495.
- [16] X. Guo, P. Wei, Effects of initial stress on the reflection and transmission waves at the interface between two piezoelectric half spaces, *Int. J. Solids Struct.* 51 (2014) 3735–3751.
- [17] M. Shams, Effect of initial stress on Love wave propagation at the boundary between a layer and a half-space, *Wave Motion* 65 (2016) 92–104.
- [18] A. Singhal, S.A. Sahu, S. Chaudhary, Approximation of surface wave frequency in piezo-composite structure, *Compos. Part B Eng.* 144 (2018) 19–28.
- [19] N. Haskell, The dispersion of surface waves on multilayered media, *Bull. Seismol. Soc. Am.* 43 (1953) 17–34.
- [20] M. Lowe, Matrix techniques for modeling ultrasonic waves in multilayered media, *IEEE Trans. Ultrason. Ferroelectr. Freq. Control* 42 (1995) 525–542.
- [21] W.Q. Chen, C.F. Lü, Z.G. Bian, A mixed method for bending and free vibration of beams resting on a Pasternak elastic foundation, *Appl. Math. Model.* 28 (2004) 877–890.
- [22] H. Zheng, Z. Yang, C.H. Zhang, M. Tyrer, A local radial basis function collocation method for band structure computation of phononic crystals with scatterers of arbitrary geometry, *Appl. Math. Model.* 60 (2018) 447–459.
- [23] S. Biswas, S.M. Abo-Dahab, Effect of phase-lags on Rayleigh wave propagation in initially stressed magneto-thermoelastic orthotropic medium, *Appl. Math. Model.* 59 (2018) 713–727.
- [24] L. Wang, S.I. Rokhlin, Stable reformulation of transfer matrix method for wave propagation in layered anisotropic media, *Ultrasonics* 39 (2001) 413–424.
- [25] F. Takali, A. Njeh, D. Schneider, M.H. Ben Ghazlen, Surface acoustic waves propagation in epitaxial ZnO/alpha-Al2O3 thin film, *Acta Acust. United Acust.* 98 (2012) 223–231.
- [26] J. Wang, Y. Shen, Numerical investigation of ultrasonic guided wave dynamics in piezoelectric composite plates for establishing structural self-sensing, *J. Shanghai Jiaotong Univ. (Science)* 23 (2018) 175–181.

- [27] J.E. Lefebvre, V. Zhang, J. Gazalet, T. Gryba, Conceptual advantages and limitations of the Laguerre polynomial approach to analyze surface acoustic waves in semi-infinite substrates and multilayered structures, *J. Appl. Phys.* 83 (1998) 28–34.
- [28] J.G. Yu, F.E. Ratolojanahary, J.E. Lefebvre, Guided waves in functionally graded viscoelastic plates, *Compos. Struct.* 93 (2011) 2671–2677.
- [29] B. Zhang, J.G. Yu, X.M. Zhang, P.M. Ming, Complex guided waves in functionally graded piezoelectric cylindrical structures with sectorial cross-section, *Appl. Math. Model.* 63 (2018) 288–302.
- [30] C. Othmani, S. Dahmen, A. Njeh, M.H. Ben Ghazlen, Investigation of guided waves propagation in orthotropic viscoelastic carbon-epoxy plate by Legendre polynomial method, *Mech. Res. Commun.* 74 (2016) 27–33.
- [31] C. Othmani, F. Takali, A. Njeh, M.H. Ben Ghazlen, Study of the influence of semiconductor material parameters on acoustic wave propagation modes in GaSb/AlSb bi-layered structures by Legendre polynomial method, *Phys. B Condens. Matter* 496 (2016) 82–91.
- [32] C. Othmani, F. Takali, A. Njeh, M.H. Ben Ghazlen, Numerical simulation of Lamb waves propagation in a functionally graded piezoelectric plate composed of GaAs-AlAs materials using Legendre polynomial approach, *Optik* 142 (2017) 401–411.
- [33] C. Othmani, A. Njeh, M.H. Ben Ghazlen, Influences of anisotropic fiber reinforced composite media properties on fundamental guided wave mode behavior: a legendre polynomial approach, *Aerospace Sci. Technol.* 78 (2018) 377–386.
- [34] X. Cao, J. Shi, F. Jin, Lamb wave propagation in the functionally graded piezoelectric piezomagnetic material plate, *Acta Mech.* 223 (2012) 1081–1091.
- [35] H. Calás, R. Rodriguez-Ramos, J.A. Otero, L. Leija, A. Ramos, G. Monsivais, Dispersion curves of shear horizontal wave surface velocities in multilayer piezoelectric systems, *J. Appl. Phys.* 107 (2010) 044511.
- [36] J. Chen, E. Pan, H. Chen, Wave propagation in magneto-electro-elastic multilayered plates, *Int. J. Solids Struct.* 44 (2007) 1073–1085.
- [37] Y.Q. Guo, W.Q. Chen, Y.L. Zhang, Guided wave propagation in multilayered piezoelectric structures, *Sci. China Ser. G Phys. Mech. Astron.* 52 (2009) 1094–1104.
- [38] G. Nie, J. Liu, M. Li, in: Effect of an Initial Stress on SH-type Guided Waves Propagating in a Piezoelectric Layer Bonded on a Piezomagnetic Substrate, 48, Tech Science Press, 2015, pp. 133–145.
- [39] M. Mahanty, A. Chattopadhyay, P. Kumar, A.K. Singh, Effect of initial stress, heterogeneity and anisotropy on the propagation of seismic surface waves, *Mech. Adv. Mater. Struct.* 0 (2018) 1–12.